PLOS WATER

RESEARCH ARTICLE

Desiccation of ecosystem-critical microbialites in the shrinking Great Salt Lake, Utah (USA)

Carie Frantz[1,2]*, Cecilia Gibby[2], Rebekah Nilson[1], Cole J. Stern[1], Maggie Nguyen[1], Cody Ellsworth[2], Hank Dolan[3], Alvin Sihapanya[4], Jake Aeschlimann[5], Bonnie K. Baxter[4]

1 Department of Earth and Environmental Sciences, Weber State University, Ogden, UT, United States of America, **2** Environmental Science Program, Weber State University, Ogden, UT, United States of America, **3** Northern Utah Academy for Math, Engineering and Science, Ogden, UT, United States of America, **4** Great Salt Lake Institute, Westminster University, Salt Lake City, UT, United States of America, **5** Department of Microbiology, Weber State University, Ogden, UT, United States of America

* cariefrantz@weber.edu

Citation: Frantz C, Gibby C, Nilson R, Stern CJ, Nguyen M, Ellsworth C, et al. (2023) Desiccation of ecosystem-critical microbialites in the shrinking Great Salt Lake, Utah (USA). PLOS Water 2(9): e0000100. https://doi.org/10.1371/journal.pwat.0000100

Editor: Sanja Gottstein, University of Zagreb Faculty of Science: Sveuciliste u Zagrebu Prirodoslovno-matematicki fakultet, CROATIA

Received: February 3, 2023

Accepted: August 7, 2023

Published: September 12, 2023

Peer Review History: PLOS recognizes the benefits of transparency in the peer review process; therefore, we enable the publication of all of the content of peer review and author responses alongside final, published articles. The editorial history of this article is available here: https://doi.org/10.1371/journal.pwat.0000100

Data Availability Statement: All data, including photographs and photomicrographs used for analyses in this paper are archived through Open

Abstract

Great Salt Lake hosts an ecosystem that is critical to migratory birds and international aquaculture, yet it is currently threatened by falling lake elevation and high lakewater salinity resulting from water diversions in the upstream watershed and the enduring megadrought in the western United States. Microbialite reefs underpin the ecosystem, hosting a surface microbial community that is estimated to contribute 30% of the lake's primary productivity. We monitored exposure, desiccation, and bleaching over time in an area of microbialite reef. During this period, lake elevation fell by 1.8 m, and salinity increased from 11.0% to 19.5% in open-water portions of the outer reef, reaching halite saturation in hydrologically closed regions. When exposed, microbialite bleaching was rapid. Bleached microbialites are not necessarily dead, however, with communities and chlorophyll persisting beneath microbialite surfaces for several months of exposure and desiccation. However, superficial losses in the mat community resulted in enhanced microbialite weathering. In microbialite recovery experiments with bleached microbialite pieces, partial community recovery was rapid at salinities $\leq$ 17%. 16S and 18S rRNA gene sequencing indicated that recovery was driven by initial seeding from lakewater. At higher salinity levels, eventual accumulation of chlorophyll may reflect accumulation and preservation of lake material in halite crusts vs. true recovery. Our results indicate that increased water input should be prioritized in order to return the lake to an elevation that submerges microbialite reefs and lowers salinity levels. Without quick action to reverse diversions in the watershed, loss of pelagic microbial community members due to sustained high salinity could prevent the recovery of the ecosystem-critical microbialite surface communities in Great Salt Lake.

Introduction

Great Salt Lake: A globally-important ecosystem threatened by water overuse

Saline lakes around the world are facing a "desiccation crisis": threatened by water overuse and climate change, with wide-ranging consequences to regional and hemispheric ecosystems,

Science Framework at https://osf.io/t6w5e/. Scripts used for image and data processing are archived under DOI:10.5281/zenodo.7502617. Sequences were deposited to NCBI's SRA (https://www.ncbi.nlm.nih.gov/sra) under BioSample accession SAMN32545145–SAMN32545168.

Funding: This work was supported by National Science Foundation (nsf.gov) EAR # 1826869 and EAR # 1801760 to CF. The latter grant also funded the Geoscience Education Targeting Underrepresented Populations (GETUP) Summer Research Experience program at Weber State University, which supported CG, RN, MN, CE, CS, and other students mentioned in the acknowledgements. CG & RN received additional support for their work on this project from the Weber State University Office of Undergraduate Research and Department of Earth and Environmental Sciences. AS was supported by Utah NASA Space Grant #80NSSC20M0103 and a Ronald E. McNair Scholars grant #P217A220138 to Westminster College. BB was supported in part from a grant from the State of Utah, Department of Natural Resources, Division of Forestry, Fire, and State Lands. The funders had no role in study design, data collection and analysis, decision to publish, or preparation of the manuscript.

Competing interests: The authors have declared that no competing interests exist.

air quality, weather patterns, economic activities, and more [1–3]. In this paper, we present a case study of the largest terminal lake in the Western hemisphere: Great Salt Lake, in northern Utah within the arid Great Basin, which has experienced a sustained decline in lake level driven by human overconsumption in its watershed (Fig 1) [1].

Great Salt Lake comprises not only the hypersaline open water but also distinct habitats along a salinity gradient, including fresh- to brackish-water estuaries and wetlands where rivers enter the lake, and expansive mudflats and playas. The main body of the lake is segmented by a rail causeway, which isolates the salt-saturated north arm (Gunnison Bay) from the south arm (Gilbert Bay), which encompasses our study site. The south arm supports a relatively simple but significant food web (Fig 2A); Great Salt Lake is a hemispherically important ecosystem [4] that supports millions of resident and migratory birds [5, 6] and a brine shrimp industry that harvests cysts used as feed in global aquaculture [7]. The lake is a hypersaline Cl-Na-SO_4-Mg-dominated system [8, 9] with chemical and biological factors contributing to its "carbonate factory" [10] despite moderate modern pH values; carbonate deposits include oolitic sand, organic-rich carbonate mud, and mounded reef-forming microbialites [11, 12].

Great Salt Lake is currently threatened by a rapid decline in lake levels and consequent increase in salinity. Layered onto normal decadal cycles in precipitation [15], its watershed has been impacted by the megadrought that has gripped the western United States since 2000, which has been worsened by anthropogenic climate change [16]. An even greater threat to the lake, however, has been the overuse and diversion of the waters that would otherwise feed Great Salt Lake for agricultural, industrial, and municipal uses. Such consumptive water diversions are estimated to have reduced the lake's volume by >60% [17]. As a result, the lake has shrunk to historic low levels in the past decade (Fig 1E and 1F), following a pattern of water overuse leading to lake demise seen in ecologically-important saline lakes around the world [1, 5]. Water overuse in Great Salt Lake's watershed has substantially impaired the lake's resilience to future changes in regional hydroclimate [18]. It has become clear that, without an overhaul of water use policy and practice in the watershed, the lake could soon be lost [19].

Great Salt Lake's ecosystem-critical microbialites in peril

Low lake levels and consequent shoreline shift has exposed hundreds of square kilometers of microbialite mounds, which occur in extensive reefs [13] in Great Salt Lake's near-shore environments and benthos. Microbialites, carbonate mounds formed by interactions of microbes with the lake's chemical environment, are of academic interest as analogues for economically important hydrocarbon reservoirs [11] and paleoenvironmental records [12, 20, 21]. Microbialites are not unique to Great Salt Lake; indeed, other lakes threatened by modern lake level decline are home to similar structures, including microbially-influenced carbonate mounds in several other lakes in the Western flyway, Australia's Lake Clifton in Australia, Ethiopia and Djibouti's Lake Abhe, and the giant microbialites of Turkey's Lake Van [22–24].

Although typically viewed as relics—geobiologic curiosities that provide a window into Earth's deep past and life's evolution—microbialites are beginning to gain appreciation for their role in supporting modern ecosystems (e.g., [25, 26]). Perhaps the best-studied example of this is Great Salt Lake, where it has become apparent that the lake's microbialites serve a critical function in the lake's overall ecosystem. Robust photosynthetic microbial mats (periphyton, adopting for this paper the broad definition that acknowledges the presence of a diverse community, cf. [27]) exist on the surfaces of microbialites in Great Salt Lake when conditions—primarily submergence and salinity—are favorable. The periphyton is dominated by a single genus of halophilic, coccoidal cyanobacteria, *Euhalothece* (Fig 2), although other phototrophs, including diatoms, green algae, and flagellates, can be seen associated with the mats, and the

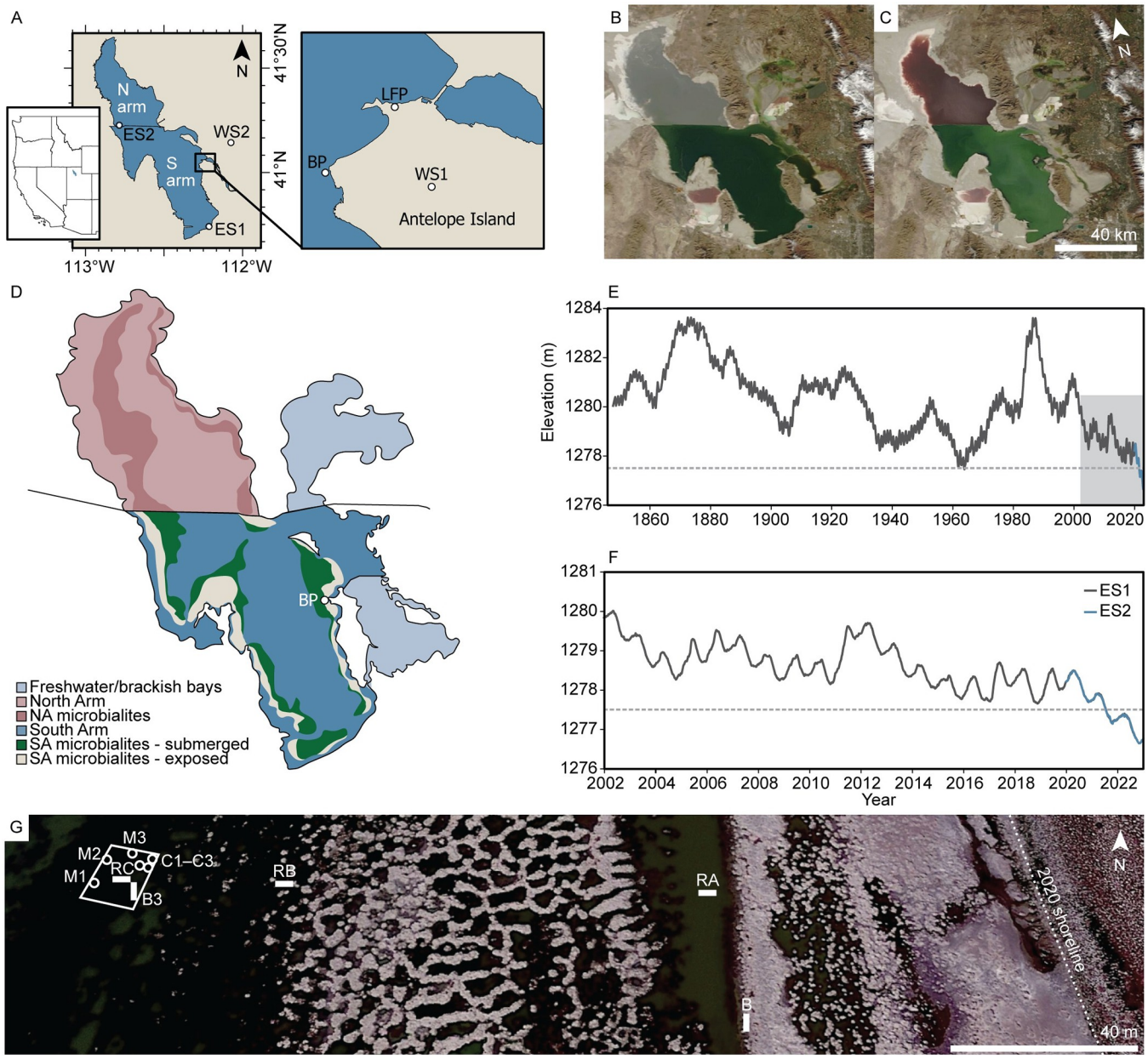

Fig 1. Great Salt Lake field sites and hydrograph. (A) Map of Great Salt Lake showing the north (N) and south (S) arms of the lake with major sites described in this paper: USGS lake elevation sites 1001000 (ES1, Saltair site) and 10010024 (ES2, Causeway site), weather station sites KUTSYRAC22 (WS1) and KUTSYRAC27 (WS2), Buffalo Point microbialite reef sites (BP), and Ladyfinger Point (LFP). Left inset shows the location of Great Salt Lake (blue) in northern Utah, USA. Right inset shows the northern tip of Antelope Island. Map baselayers are from the U.S. Geological Survey, National Geospatial Program (https://basemap.nationalmap.gov/arcgis/rest/services/USGSTopo/MapServer and https://www.sciencebase.gov/catalog/item/52c78623e4b060b9ebca5be5). (B) Satellite images of Great Salt Lake from October 29, 2012 and (C) October 28, 2022 showing the shrinking shoreline of Great Salt Lake (MODIS corrected reflectance images from NASA Worldview). (D) Map of Great Salt Lake (at 1280 m elevation) showing the approximate location and extent of submerged vs. exposed microbialite reef areas in summer 2022, after Baskin et al. [13]. (E) Lake hydrograph from 1848 to 2022; area highlighted in gray is expanded in (F). The dashed gray line in both figures shows the historical (1963) lake lowstand. (G) Detail of field sites at Buffalo Point, with logger sites as vertical bars (B and B3), recovery experiment sites as horizontal bars (RA–RC), and the microbialite monitoring quad with monitored (M1–M3) and cored (C1–C3) microbialites. The 2020 shoreline is also shown as a dashed line. The underlying aerial view (from Google Earth) shows the site in May 2022, with bright areas showing exposed, desiccated microbialites.

https://doi.org/10.1371/journal.pwat.0000100.g001

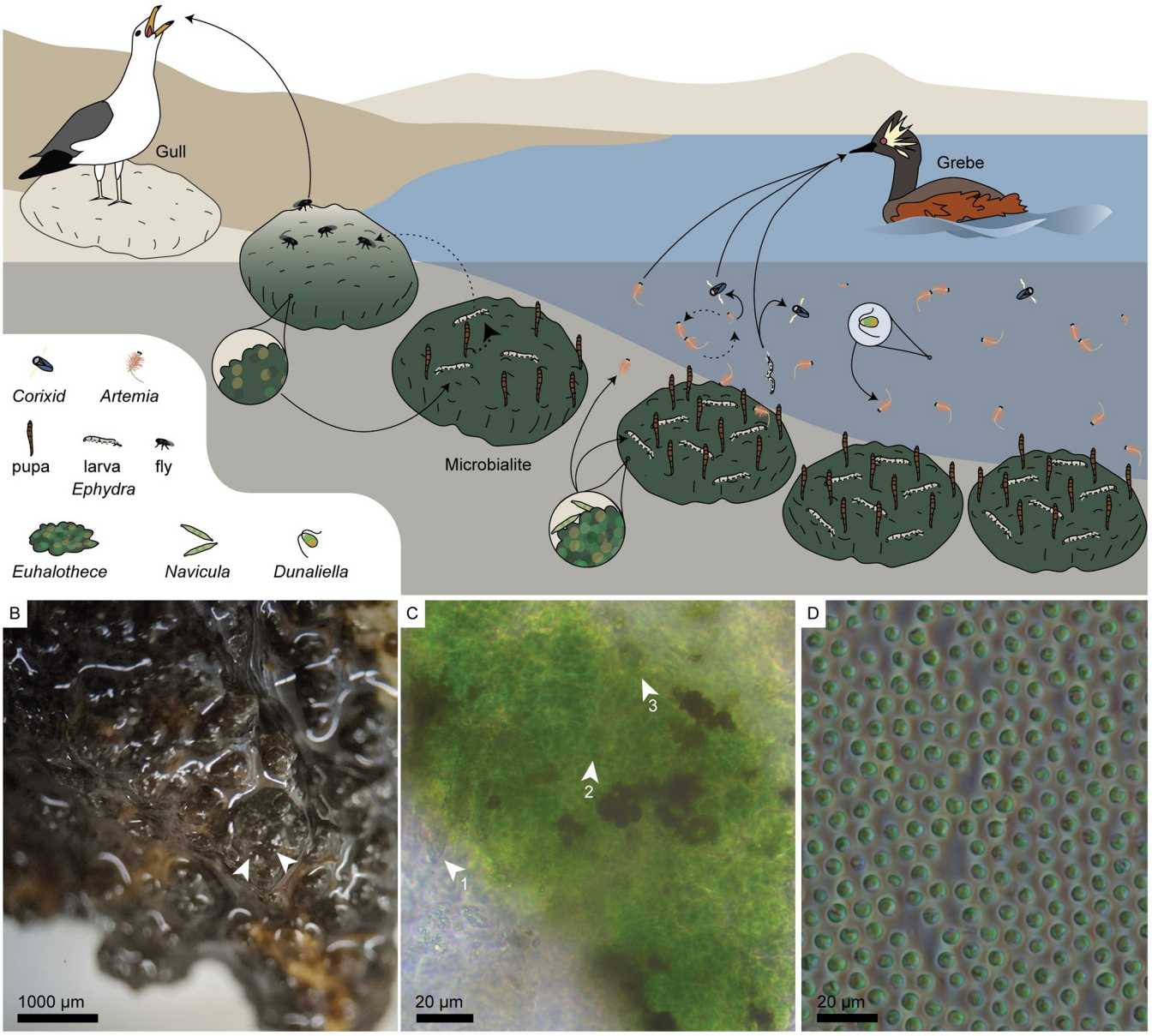

Fig 2. Great Salt Lake's microbialite-supported ecosystem. (A) Simplified ecosystem diagram of Great Salt Lake's south arm, illustrating the importance of the lake's microbialites and the effect of microbialite exposure. Dashed arrows represent life cycle stages, solid arrows represent consumption. After Baxter (2018) [63] & Belovsky et al. (2011) [35]. (B) Stereo-photomicrograph of a Great Salt Lake microbialite piece imaged at 10x showing a healthy periphyton community, with three-dimensional clumps of *Euhalothece* bound by extracellular polymers, and white points of carbonate highlighted with arrows. Sample collected from Site B on July 7, 2020. (C) Phase contrast photomicrograph of a healthy microbialite periphyton community sample imaged at 400x magnification. The greenish mass is a clump of *Euhalothece*. Also visible in association with the *Euhalothece* mat are a pennate diatom (arrow 1), filamentous organism (arrow 2), and green alga (arrow 3). Sample was collected October 10, 2019 from Site B. (D) Positive phase and differential interference contrast photomicrograph imaged at 1000x magnification of *Euhalothece* culture from a Great Salt Lake microbialite sample collected in 2019 at Antelope Island State Park [**14**].

https://doi.org/10.1371/journal.pwat.0000100.g002

mat community is taxonomically and functionally diverse [12, 28, 29]. Microbialite periphyton conservatively contribute one third of the primary production in Great Salt Lake [30, 31].They are the primary food source for brine fly (*Ephydra* spp.) larvae [32, 33], as well as a seasonally important food source for the lake's economically important brine shrimp (*Artemia franciscana*) [7, 33]. Additionally, microbialites, which are presumably built by carbonate production

facilitated by their periphyton [28], offer stable oases in the shifting oolitic sands and carbonate mud that compose most of the Great Salt Lake benthos. This makes them crucial habitat for *Ephydra* larvae, which depend on the microbialites for both food and pupation habitat [32, 33]. The organisms that microbialite periphyton support feed in turn feed millions of birds that depend on the lake ecosystem [5, 30, 32–36] (Fig 2A). Lake level fall is subjecting microbialites and their periphyton to desiccation.

In autumn 2022, roughly 40% of the lake's microbialites were subaerially exposed (Fig 1D, [13, 37]) and desiccated (Figs 1G and 3), representing a substantial loss of productivity. A critical question for the management of Great Salt Lake and its associated watershed is how effectively and under what conditions the microbialite periphyton communities persist. If policies are enacted that allow lake levels to rebound, do microbialite periphyton communities recover their ecosystem function? We investigated these questions during two successive summers where historic lake lowstands were reached and exceeded (2021 and 2022); this paper presents the findings along with other recent data on Great Salt Lake's microbialite periphyton communities.

Materials and methods

Field sites, time series data logging, and sample collection

The work described in this study focused on a microbialite reef on the northern end of Antelope Island in Great Salt Lake (Fig 1). GPS coordinates of all measurement and sample locations are provided in S1 Table. Time series water pressure, temperature, and downwelling irradiance were measured every 15 minutes collected using data loggers (temperature/pressure: HOBO U20L, light/temperature: HOBO MX2202, Onset Computer Corporation) attached to a PVC pipe anchored to the lake bed. In March 2019, the instrument site was placed in 0.9 m deep water in a microbialite reef ~75 m from that date's shoreline (Site B; Fig 1G). In August 2021, Site B became subaerially exposed (Fig 3A) and the logger pipe was moved to a deeper site ~150 m farther lakeward from the 2019 shore (Site B3; Fig 1G). In addition, manual water depth, visibility, salinity (using a handheld 0–28% refractometer with automatic temperature compensation; measurements are reported as a % by mass), density (using a brewing hydrometer), and temperature (using a digital aquarium thermometer) measurements were collected monthly to seasonally, along with microbialite surface observations. Lake elevation data were obtained from two U.S. Geological Survey monitoring sites in the lake's South Arm (Fig 1A) in order to provide a continuous record of lake elevation during the period of our study: one near Saltair (ES1: Station 10010000, the standard site for Great Salt Lake south arm elevation measurements, which had an interruption in data collection from 2022-09-28 to 2022-12-14 due to historic lake level fall), and the other on the railroad causeway (ES2: Station 10010024, which operated from 2020-06-08 onwards) [38]. Multiple manual field measurements of site water depths at each site were then used to determine depth offsets vs. lake level (i.e., site elevation). During dates when both ES1 and ES2 recorded data, daily mean values at the two sites were averaged for inferring water depth changes at our field sites.

Weather data

Weather data for 2019–November 2020 was obtained from a station on Antelope Island, located 4 km from the field site and operated by Antelope Island State Park (WS1: KUTSYRAC22, Ambient Weather WS-2090; Fig 1A); the station was non-operational beginning in November, 2020. Data for nearby stations available on WeatherUnderground (wunderground.com) were analyzed to find a new station with values consistent with those measured at KUTSYRAC22; for the full analysis see the file in the Open Science Framework data archive for this

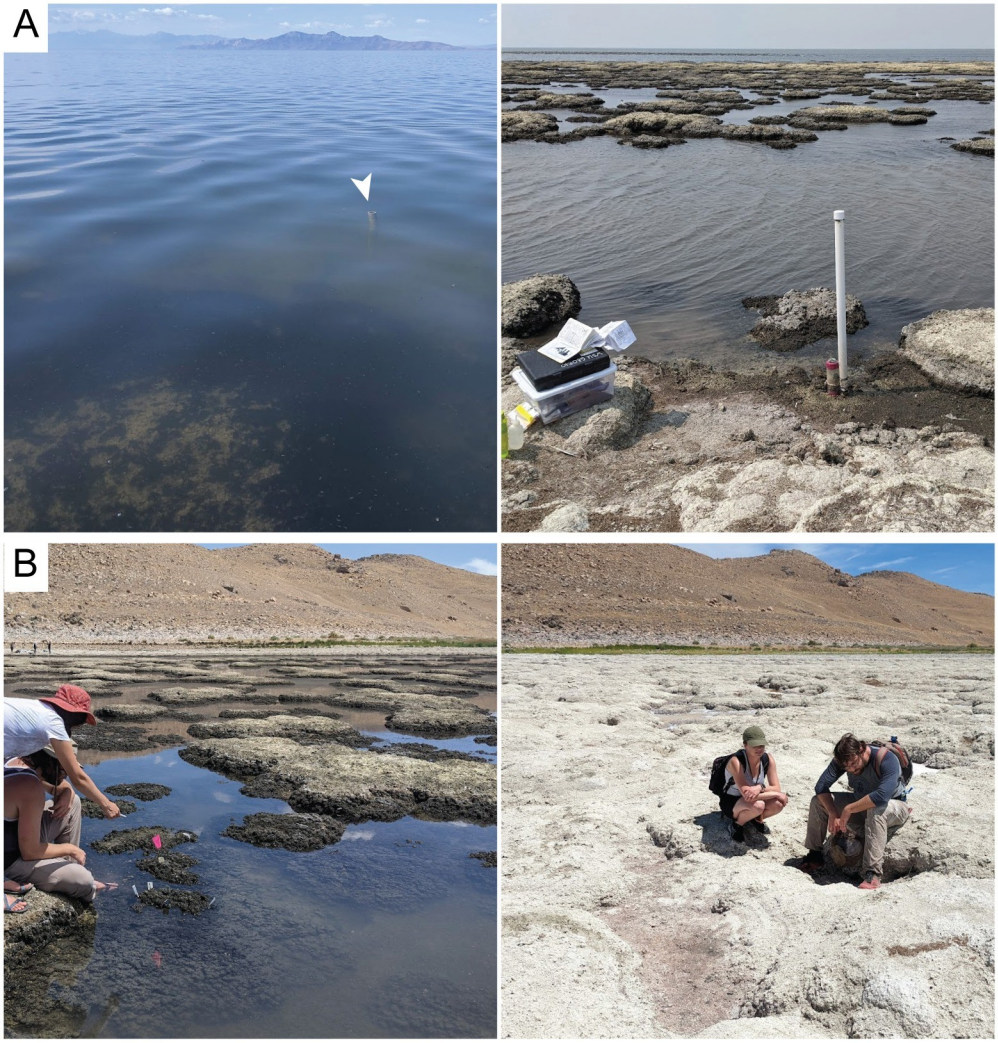

Fig 3. Time series photographs from Buffalo Point field sites showing the effects of lake level fall. (A) Site B instrument pipe in July 2019 (left; top of pipe highlighted with arrow) vs. August 2021 (right). (B) Site B3 microbialite site in July 2021 (left) vs. July 2022 (right).

https://doi.org/10.1371/journal.pwat.0000100.g003

study (hereafter referred to as OSF archive). The station with the best coverage and closest similarity to KUTSYRAC22 was determined to be a private station located 14 km from the field site (WS2: KUTSYRAC27, Ambient Weather WS-2902; Fig 1A), with publicly available data retrieved and used in this study with permission from the station owner. For analytical purposes, measured weather values were averaged when data from both sites were available.

Microbialite field monitoring & core sampling

In addition to general observations collected during the long-term monitoring work, detailed systematic monitoring of microbialites at the study sites was conducted from July 27–August 17, 2021 and July 12–August 2, 2022 as part of the Weber State University GETUP (Geoscience Education Targeting Underrepresented Populations) Summer Research Experience program. Microbialites monitored in summer 2022 were additionally visited and sampled sporadically until October 20, 2022. For this work, microbialites were flagged for repeat photography and

sampling. In 2022, monitored microbialites (in addition to logger Site B3 and recovery experiment Site RC) were located within a roped-off rectangle (quad) to protect them from foot traffic, as the lake's microbialites are currently unprotected. Each flagged microbialite was photographed during each visit, and the location of different colored bands on the surface of each microbialite were measured using a homemade surveying device (Fig S1.1 in S1 Appendix): the vertical distance of the band from the water surface, corrected for fluctuating lake elevation, was used to compare band height across dates. The vertical distance from the sediment/water interface was also measured, however the soft and mobile nature of the sediment surrounding the microbialites made measurement from the water surface the more reliable measurement.

In 2022, core samples from microbialite tops were collected using 50 mL syringes with the tapered tip cut off, producing a coring tube that could be pushed by hand directly into the incompletely-lithified surfaces of the microbialites, to a depth of up to 4–7 cm. Cores were then extracted using the syringe plunger onto core cradles with a scale, and photographed. The 3–7 cm cores were sectioned in the field into three roughly equal 1–2 cm top, middle, and bottom (deep) sections using a sterile scalpel, then stored in sterile 15 mL centrifuge tubes on ice for transport to the lab. For downstream analyses, collected sections were coded based on their original depth within the microbialite as belonging to one of several horizons, with horizon T capturing the uppermost 0–1 cm, horizon M capturing 1–2.5 cm, and horizon B capturing 2.5–4 cm (see S1 Appendix for details). Back in the lab, core subsections were ground to a paste with a sterilized mortar & pestle to homogenize, then aliquoted for microscopy and chlorophyll extraction as described below.

Recovery experiments

Recovery experiments involved submerging pieces of a desiccated microbialite back into lakewater, incubating for varying lengths of time, and recovering them for measurements of community regrowth. The desiccated microbialite (t_0 control) was collected in October 2016 from the beach at Ladyfinger Point (Fig 1A) at roughly 1278.6 m elevation, indicating that it had been subaerially exposed for at least two years at the date of collection, after which it sat undisturbed and dry on a laboratory windowsill until its use in this experiment. The t_0 control microbialite was broken into 1–7 g pieces, which were placed into individual nylon mesh bags (mesh size = 350 μm) that were attached to submerged PVC anchors (Fig S1.3 in S1 Appendix) such that the samples hung suspended in the middle of the water column at the start of the experiment. In 2021 (September 27–November 12), experiments were run at two sites: Site RA (near the edge of a microbialite reef with significant water movement), and Site RB (in the middle of a reef surrounded by microbialites with healthy periphyton), both of which had water depths to sediment of ~ 20 cm, and samples were suspended at ~ 10 cm beneath the water surface. Triplicate samples were collected at timepoints from 10–40 days. The experiment was repeated in 2022 (September 27–November 12) at Site RC (adjacent to logger instrument Site B3 in the middle of a different, initially healthy microbialite reef), at a water depth to sediment of ~ 40 cm, and samples were suspended at ~ 30 cm beneath the water surface. Triplicate samples at Site RC were collected at timepoints from 0–100 days. All three sites were hydrologically connected (open) to south arm lake water at the beginning of the experiments, however, Site RC became hydrologically closed during the course of the experiment due to rapid lake level decline.

In 2021, samples collected at each timepoint were subsampled in the field for pigment and DNA extractions. Pigment subsamples were collected with surrounding lakewater in sterile 1.5 mL centrifuge tubes wrapped in electrical tape to minimize light exposure. DNA subsamples

were collected by first swabbing an area of each sample and mixing the swab in DNeasy PowerSoil kit (Qiagen, Cat. # 12888–50) bead tubes that had been prepared with kit lysis solution. Then, a ~ 5 mm solid piece of each sample was also broken off using sterile tweezers and added to the same bead tube. Both pigment and DNA subsamples were flash-frozen on dry ice and stored frozen for transport. Back in the lab, DNA samples were thawed, vortexed for 5 minutes, and stored frozen at -20˚C until extracted following kit protocols (see S1 Appendix for additional details). Pigment samples were processed immediately following the protocols described below.

In 2022, instead of processing samples in the field, samples were stored in sterile centrifuge tubes placed on ice for transport, and processed in the lab. Whole samples were then ground and processed following the pigment extraction and microscopy protocols in the same manner described for the core samples, and DNA extractions were performed using the same protocol as for the 2021 recovery experiment samples.

Laboratory desiccation experiments

A submerged microbialite was collected near Site B3 in July, 2022, then placed in an incubator at 30˚C with one full-spectrum LED lamp (24W 3500 K full-spectrum lamp, Juhefa, Cat. # B08S7VSX6) and one UVA/UVB CFL lamp (23W 6500 K UVA/UVB lamp, Lucky Herp, Cat. # B082DYBQLL); spectra are shown in Fig S1.4 in S1 Appendix. The microbialite was allowed to desiccate for several days to weeks, and rinsed with distilled water at intervals between 6–52 days to simulate rain events. Microbialite surface coloration was measured immediately before and after rinsing events and periodically thereafter. Photographs were taken alongside a color card under standardized light conditions in order to measure surface coloration using the method described below. In addition, the dry mass of the microbialite was measured to assess removal of surface carbonate (weathering) during rinsing events.

Color analysis

Microbialite surface coloration—specifically, the relative amount of green—was measured as an indicator of surface pigmentation for field microbialites and the microbialite in the laboratory desiccation experiment, with lack of green indicating surface bleaching. To quantify coloration, photographs were taken of microbialite surfaces alongside a standard color card (Pixel Perfect 24-Color Standard Calibration Chart). Color thresholding was done using the public-domain image processing software ImageJ (https://imagej.nih.gov), and the thresholded images were then used to quantify the green pixels in an image, with a full protocol described in S1 Appendix.

Microscopy

Core and recovery experiment samples collected for microscopy were weighed (~0.2 g dry mass), vortexed with 1 mL of 2% PBS-buffered formaldehyde to fix, and stored at 4˚C. For both phase contrast and confocal laser scanning microscopy (CLSM), wet mount slides were prepared from ~60–100 μL of sample that had been vortexed to suspend solid material, using clear nail polish to seal coverslips to prevent water evaporation and salt precipitation. Bright-field and phase contrast microscopy photomicrographs were collected using an Accu-Scope EXC-500 with an Excelsis MPX-16C camera and CaptaVision software. For confocal laser scanning microscopy (CLSM), 4',6-diamidino-2-phenylindole (DAPI, 1 μL of 1 μg·mL-1 stock in sterile, nuclease-free water; Thermo ScientificTM Cat. # 62248) and calcein (1 μL of 100 μg·mL-1 stock in sterile, nuclease-free water; Invitrogen Cat. # C481) fluorescent probes were added to the fixed sample prior to fixing cover slips, and fixed slides were stored in a dark

box prior to analysis to prevent photobleaching. CLSM photomicrographs were imaged using an Olympus FV3000 with the following channels: DAPI (for staining DNA), ex = 405 nm, em = 430–480 nm; calcein (highlighting bound Ca^{2+} and Mg^{2+}, which can be used to image polymers and biogenic carbonate), ex = 488 nm, em = 500–540 nm; and chlorophyll, ex = 514 nm, em = 550–600 nm (full settings used for imaging are in S1 Appendix). For both phase contrast microscopy and CLSM, ten random photomicrographs were collected at 200x magnification for relative color/fluorescence analysis, and interesting features were photographed at various magnification; protocols for color/fluorescence analysis are described in detail in S1 Appendix. The *Euhalothece* culture in Fig 2D was imaged using an Olympus BX51 microscope using a DP27 5 MP capture card mounted on a U-TV1XC adaptor; positive phase contrast and DIC were achieved by pairing an Olympus CX-PCD Phase Contrast condenser on Ph3 setting and Nomarsky DIC filter with a 100x objective.

Chlorophyll extractions

Chlorophyll extraction protocols used in 2021 and 2022 differed slightly in response to changes in equipment availability. In 2021, pigment samples were extracted by grinding solid samples to a powder using a sterile mortar and pestle, weighing the powder, then extracting overnight in 5 mL chilled, 100% acetone at 4˚C in 9 mL glass test tubes. The next day, the glass tubes were centrifuged inside 15 mL polypropylene centrifuge tubes for 5 minutes at 3000 g to sediment solids. The supernatant, containing polar pigments, was scanned in a 3.5 mL quartz cuvette (Vernier) from 500–800 nm at 1 nm spectral resolution and 0.1 s·λ-1 averaging using a UV-VIS spectrophotometer (Cary 60, Agilent).

In 2022, solid samples were weighed, added to 4˚C chilled 90% acetone in 1.5 mL opaque black polypropylene tubes (Argos Technologies), vortexed 5 seconds to mix, and polar pigments were extracted overnight at 4˚C. Prior to measurement, samples were again vortexed, then centrifuged at 1000 g to sediment solids. Supernatant containing pigments was then scanned in a 400 μL quartz cuvette from 350–1000 nm at 1 nm spectral resolution and 0.1 s averaging using the UV-VIS spectrophotometer. Samples with dense concentrations of pigments (with peak absorbance readings > 2.0) were diluted with chilled 90% acetone prior to reading.

Chlorophyll *a* concentrations were then quantified using the equation described in Ritchie (2008), correcting for dilutions and normalizing to extracted sample mass. Values are reported as mg extractable chlorophyll *a* per gram of dry microbialite sample (mg/g).

DNA extraction, sequencing, and analysis

DNA extractions were performed using a DNeasy PowerSoil kit (Qiagen, Cat. # 12888–50), and extracted DNA was quantified fluorometrically (Qubit 2.0 Fluorometer, Life Technologies) with a high-sensitivity, double-stranded DNA analysis kit (ThermoFisher Scientific Cat # Q32851). Sample barcoding, amplification, and pooling for both 16S and 18S SSU rRNA genes was performed per Earth Microbiome Project protocols (16S: [39]; 18S: [40, 41]) by Wright Labs (Huntington, PA, USA). Amplicon sequencing was done, also by Wright Labs, using Illumina MiSeq v2 chemistry with paired-end 250 base pair reads for 16S, or 150 base pair reads for 18S. Sequences were deposited to the National Institute of Health's Sequence Read Archive (SRA) under BioSample accession SAMN32545145–SAMN32545168. Sequence analysis was performed using the Qiime2 pipeline [42]: quality-controlled amplicon sequence variants (ASVs) were taxonomically classified against the SILVA 138 database [42], then filtered prior to diversity analysis: mitochondria, chloroplasts, or unassigned sequences were removed from the 16S dataset; and bacteria, and non-microbial or contaminant sequences (vertebrata,

arthropoda, and *Entomophthora muscae*) were removed from the 18S dataset. Pipeline steps are described in detail in the S1 Appendix. Raw sequence data with linked sample metadata were archived with NCBI's SRA (https://www.ncbi.nlm.nih.gov/sra) under BioSample accession SAMN32545145–SAMN32545168. Diversity analyses done with both filtered and unfiltered data are available in the OSF archive.

Results

Depth, temperature, and salinity trends at the study site

Water depth, temperature, and salinity trends are summarized in Fig 4. Daily time series data are available in S2 Table, and raw time series data are available in the OSF archive.

Changes in manual field site water depth measurements correlated closely with lake elevation changes when field sites remained hydrologically connected to the greater lake (Fig 4A). We were therefore able to estimate site elevations of 1277.26 m at Site B, 1277.0 at Sites RA and RB, and 1276.55 at Site B3 and RC. Using logged lake elevation data, we could then estimate site water depth over time during periods when sites were hydrologically open. Manual measurements were used when sites became hydrologically closed, which resulted in faster evaporation compared to the lake as a whole. Water depth at Site B declined by 0.95 m from July 2019 to July 2021, and declined an additional 0.10 m during the three weeks of microbialite desiccation monitoring in 2021, at which point the site became dry and the instrument pipe was moved to Site B3. Although some depth variability was recorded, there was no significant decline in water depth during the 2021 recovery experiment (Sites RA and RB), with a median water depth to sediment of ~ 20 cm at both sites (with samples suspended at ~ 10 cm). Water depth declined 0.11 m at Sites B3 and RC during the three weeks of microbialite desiccation monitoring in 2022, and an additional 0.27 m during the remaining duration of the 2022 recovery experiments such that by the end of the experiment at 100 days, sample bags were at the water surface. The roped-off quad area containing instrument pipe B3, recovery experiment RC, monitored microbialites M1–M3, and cored microbialites C1–C3 became hydrologically closed toward mid-August, 2022, cut off from the greater lake by exposed microbialites.

Water temperature was strongly seasonal and mimicked trends in air temperatures (Fig 4B), ranging from -3.0˚C (measured January 3, 2022, when air temperature dropped as low as -7.9˚C) to +37.8˚C (measured July 31, 2022). Water temperatures were somewhat warmer during the 2022 microbialite monitoring season compared to the 2021 season (median temperature of 27.4˚C and 31.2˚C, respectively). Downwelling and sidewelling irradiance were also strongly seasonal (Fig 4C), and increased from 2021–2022, likely due to decreased water depth.

Total precipitation during the 2021 summer monitoring season was greater than during the 2022 monitoring season: 1.8 vs. 0.7 cm, respectively, with most of the rain during the 2021 monitoring season falling between the first and second monitoring weeks (Fig 4D). Total precipitation was also greater during the 2021 vs. 2022 recovery experiments: 9.6 vs. 5.0 cm, respectively, despite the substantially longer duration of the 2022 experiment.

Open-water salinity in the lakeward portion of the microbialite reef increased from 11.7% in July 2019 to 18.2% in July 2022, then to 19.5% in October 2022 (Fig 4E). Salinity proximal to the monitored microbialites was 16–17% during the 2021 monitoring season, 13–17% during the 2021 recovery experiments, 18–21% during the 2022 monitoring season, and 18–27% during the 2022 recovery experiments. Salinity in extensive, hydrodynamically restricted portions of the microbialite reef (including Sites B3 and RC) reached halite saturation in July 2022 (Fig 5), which became more widespread with lake elevation fall. Salinity measured using

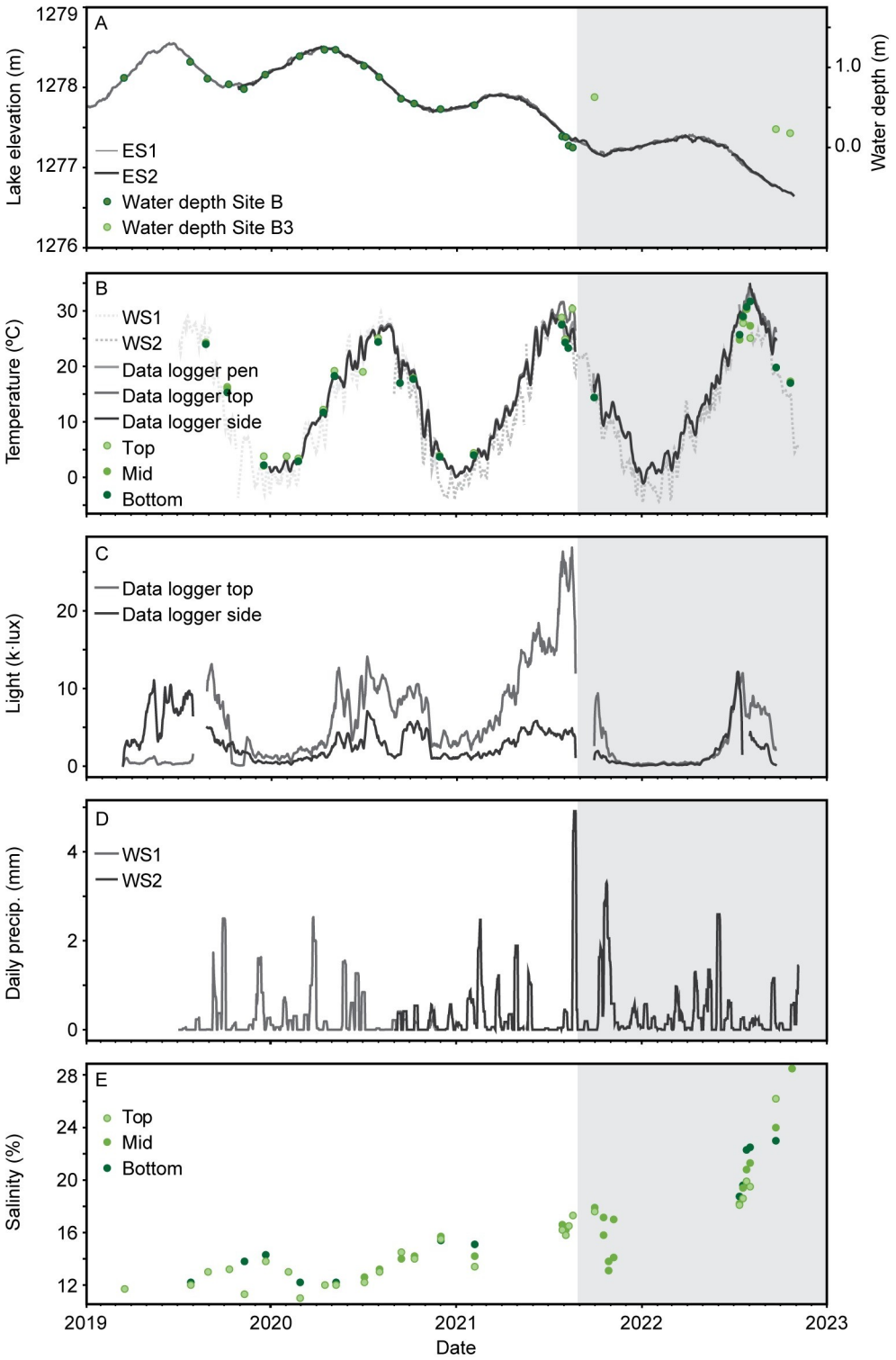

Fig 4. Environmental trends at microbialite reef field sites, 2019–2022. (A) Great Salt Lake elevation measurements (m-asl) at two USGS sites in the South Arm (left axis, lines), with manual depth measurements (right axis, circles) at Sites B and B3. (B) Air temperature (dashed lines) measured at KUTSYRAC22 (WS1) and KUTSYRAC27 (WS2), water temperature (solid lines) logged at the field site by three different data loggers, and manually measured temperatures (circles) at different water depths (water surface = top; middle depth = mid; sediment/water interface = bottom). (C) Daily mean downwelling (top) and sidewelling (side) irradiance logged at the field sites. (D)

Daily accumulated precipitation measured at station KUTSYRAC22 (WS1) and KUTSYRAC27 (WS2). (E) Water salinity measured at different water depths (water surface = top; middle depth = mid; sediment/water interface = bottom); the October 2022 point was converted from density. In all plots, the shaded gray area indicates the field site move from Site B (left) to Site B3 (right, gray).

https://doi.org/10.1371/journal.pwat.0000100.g004

different techniques were closely correlated (Fig S1.5 in S1 Appendix); we therefore use refractometer measurements (% by weight) for the remainder of this paper except values $\geq$ 25%, which were converted from lab density measurements using the equation of state from Naftz et al. [43]. For more discussion on the salinity and density measurements, see S1 Appendix.

Microbialite field monitoring and core sampling

Prolonged out-of-water (subaerial) exposure results in surficial bleaching, a process by which microbialite surfaces change color from dark green to white, and display signs of weathering (Figs 3 and 6, and S2 Fig). We observed initial stages of bleaching during both the 2021 and 2022 three-week intensive monitoring seasons (Fig 6, S1 and S2 Figs). Bleaching was quantifiable using image color analysis (Fig 6B). Quantitative results of surface monitoring are available in S3 Table. Over several-week timescales, bleaching was observed to be superficial, temporary, and influenced by water-soluble salts (especially halite); monitored microbialites re-greened following rain events (Fig 6 and S1 Fig), and samples collected were usually green just beneath the surface (< 1 cm). Indeed, microscopy revealed no obvious changes in surface samples, with *Euhalothece* clumps persisting in surface samples even in microbialites that appeared superficially bleached (S3 Fig).

Beneath the surface, microbialite communities persisted following subaerial exposure, with no statistically significant (ANOVA $p \leq 0.1$) changes in extractable chlorophyll through time at any core depth (Fig 7A). In contrast, DAPI channel fluorescence decreased over the initial 21-day monitoring period at all core depths (Fig 7B), and calcein channel fluorescence decreased somewhat in the bottom core horizon (Fig 7C). A summary of microbialite core measurements can be found in S1 File, with the raw dataset available in the OSF archive.

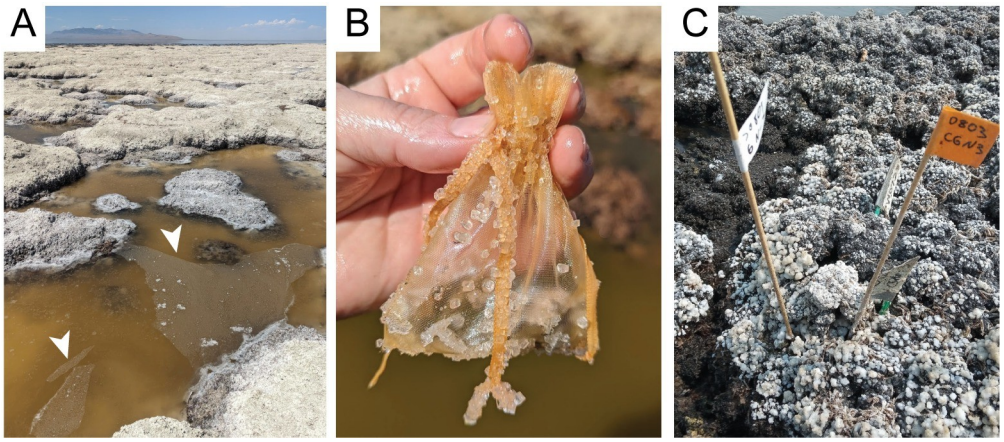

Fig 5. Field photographs showing halite saturation in closed microbialite reef areas in 2022. (A) Halite lenses (arrows) forming on a closed portion of microbialite reef within 20 m of Site B3 in July, 2022. (B) Halite crystals coating a mesh bag from the recovery experiments at Site RC in September, 2022. (C) Photograph taken August 17, 2021 showing mm-scale halite crystals (white) covering the tops of microbialites following a windy (wave action) period. Abundant brine flies and fly pupal casings (dark) are also visible in the image.

https://doi.org/10.1371/journal.pwat.0000100.g005

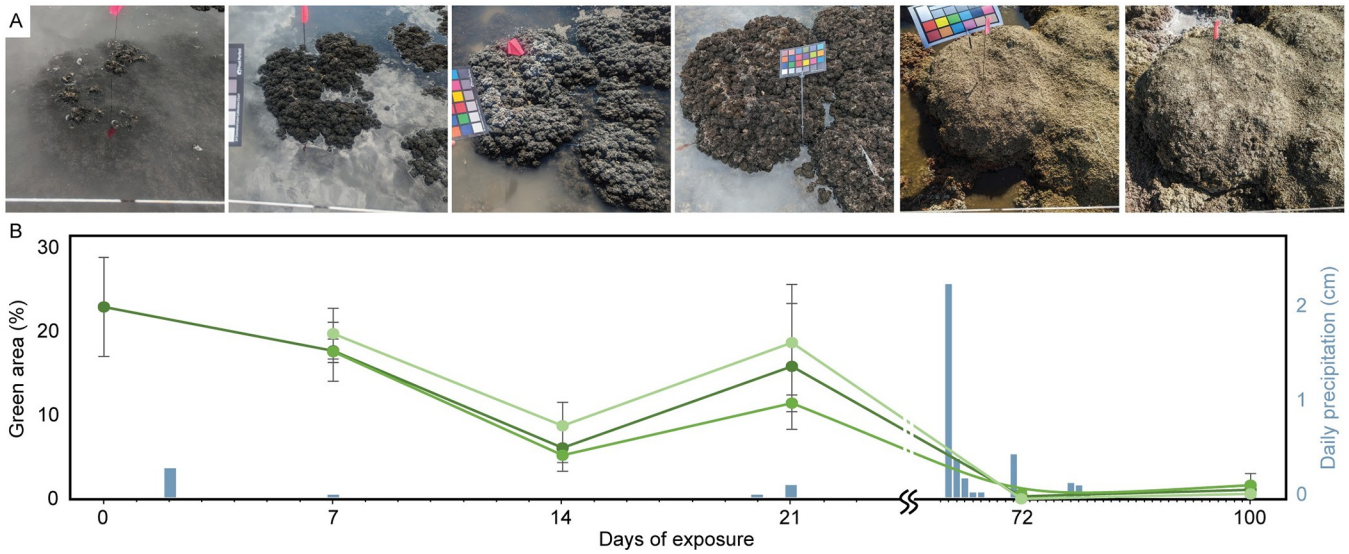

Fig 6. Visible changes of microbialite surface over 100 days of subaerial exposure. (A) Photographs of a single microbialite at Site B3 showing exposure, bleaching, and weathering during summer–autumn, 2022. Exposure times of each image align with dates notedin the graph below. (B) Surface coloration measurements of three monitored microbialites (green lines, left axis); points represent averages of three measurements in defined rectangular areas of interest (AOI) from photographs taken on each monitoring date, with standard deviations represented as error bars. Also shown are daily precipitation amounts (blue bars, right axis). Note the bright discoloration (salt precipitation) at day 14, followed by re-greening on day 21 after a light rain event, then bleaching and weathering after heavier rain on day 72, followed by continued bleaching and weathering to day 100. Tic marks are days, with labels at each sampling date.

https://doi.org/10.1371/journal.pwat.0000100.g006

Lab desiccation experiments

Lab desiccation experiments accelerated, but otherwise mimicked field observations: surficial bleaching occurred rapidly, due at least in part to the accumulation of surface salts, and was immediately reversed upon rinsing with distilled water (Fig 8). Bleaching did, however, have an impact on microbialite weathering: during each rinse, surface material (which itself re-greened upon exposure to distilled water) sloughed off, and the microbialite lost dry mass. Material that was previously resistant to weathering was easily removed following each

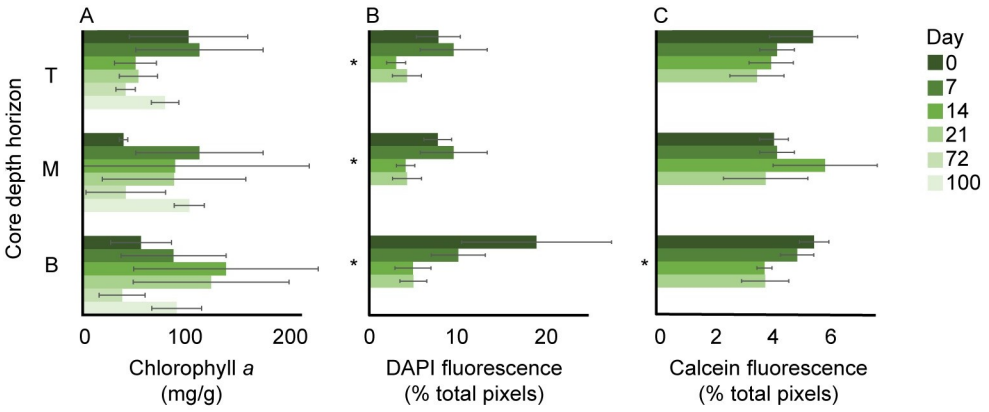

Fig 7. Microbialite core series results. Measurements from core top (T), middle (M), and bottom (B) horizons; colors represent different timepoints: 0, 7, 14, 21, 72, and 100 days. (A) Extractable chlorophyll *a*. (B) DAPI, and (C) calcein channel fluorescence in CLSM random photomicrographs as percent of total pixels. Due to resource constraints, CLSM fluorescence measurements were not done on samples after day 21. For each measurement, horizons identified as having significant change through time in ANOVA ($p \leq 0.1$) are indicated with *.

https://doi.org/10.1371/journal.pwat.0000100.g007

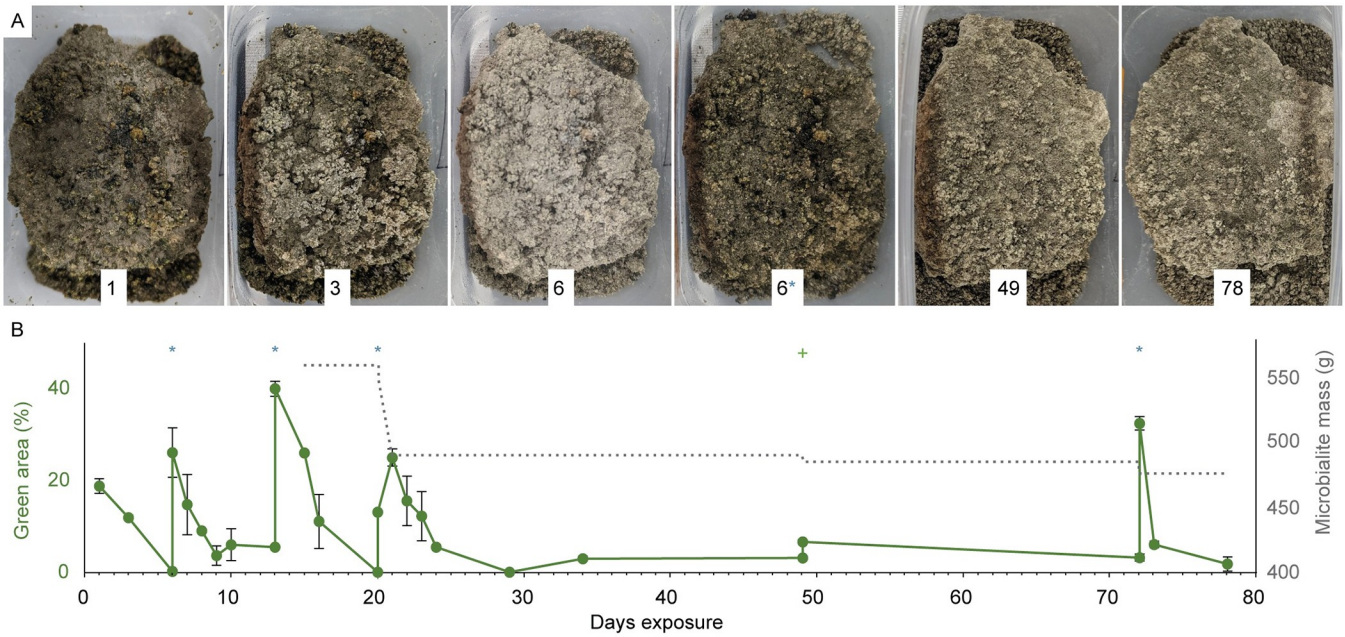

Fig 8. Lab desiccation experiment results. (A) Photograph series showing surficial changes to the microbialite, with days of exposure shown at bottom center of each image. The images for day 6 show the microbialite before and after (denoted with *) a rinse event. (B) Surface green area analysis results (green line) with points representing the average measured fraction of green pixels in three rectangular areas of interest (AOI) for each date, and standard deviations shown as error bars, overlaid on measured microbialite mass (dashed line). Disturbance events are indicated along the top: the timing of rinse events is denoted with *, and a measurement following the removal of sandy surface material on day 49 is denoted with +. Note the loss of color over time, significant regreening following all rinse events, and weathering of surface material during disruption events.

https://doi.org/10.1371/journal.pwat.0000100.g008

additional period of bleaching. Surface color measurements and masses for this experiment are available in S4 Table.

Recovery experiments

Results in 2021. In 2021, we observed exponential increases in extractable chlorophyll and DNA over the 40-days the experiment ran (Fig 9A and 9B; exponential best fit line r^2 values > 0.96 and 0.83, respectively), despite salinity levels exceeding 17% and falling water temperatures (Fig 4). In both cases, the growth rate was greater at the channel site (RA) vs. the reef interior site (RB); for chlorophyll, the doubling time was 9 days at RA, and 16 days at RB, which is on the slow end of rates reported for periphyton/biofilm recolonization of substrates in both freshwater and marine systems (e.g., [44, 45]). Extrapolating the exponential best fit lines to levels of chlorophyll *a* and DNA comparable to that of surrounding microbialites with healthy periphyton suggested a possible time to recovery in these measurements of 60–80 and 100–130 days for RA and RB, respectively (Fig 9C and 9D).

Results in 2022. The observed pattern in 2022 was different from what was observed in 2021; most notably, although eventual increases in both extractable chlorophyll *a* and DNA were observed, the trend was uneven, with r^2 values for exponential lines fit to non-zero measurements of 0.87 and 0.38, respectively (Fig 9A and 9B). The overall rates of recovery were also slower than was observed in 2021 (doubling time of 31 days for the chlorophyll measurement exponential fit). However, a substantial increase in extractable chlorophyll was observed by incubation day 72, even though halite saturation had been reached (Fig 5B), and continued to increase through day 100 of the experiment (Fig 9A). DNA concentrations also gradually increased over time. Recovery experiment measurements are summarized in S1 File, with raw data available in the OSF archive.

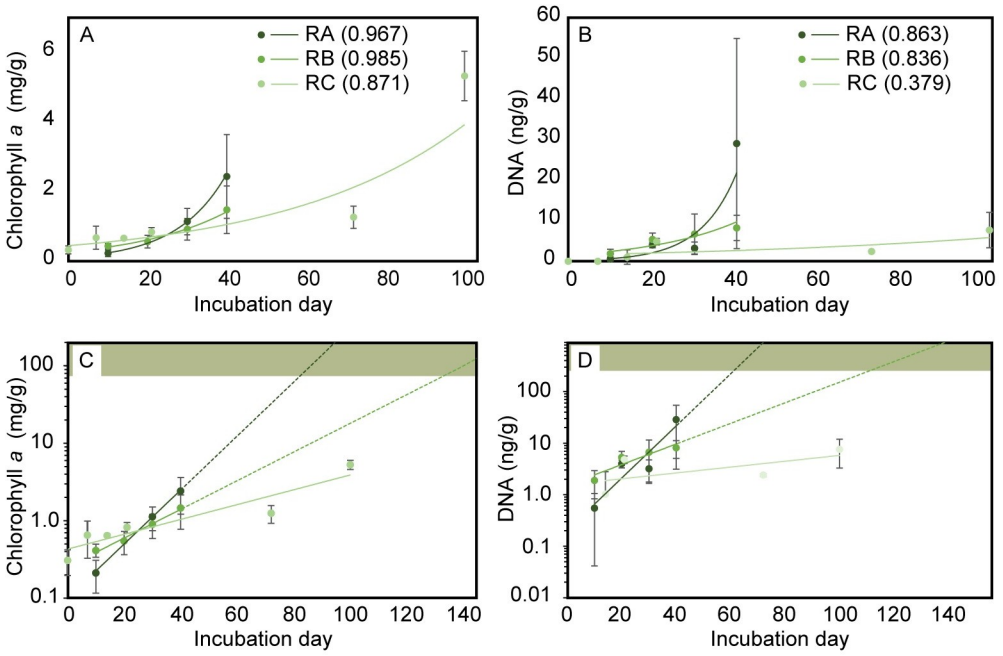

Fig 9. Recovery experiment results. The top row shows measured values of extractable chlorophyll *a* (A), and DNA (B) with exponential best-fit lines shown along with r^2 values (in parentheses next to legend entries). Exponential recovery projections (dashed lines) extrapolated from exponential best fit lines for chlorophyll *a* and DNA are shown in (C) and (D), respectively (log scale). The lower edge of the green shaded region in C & D indicates the mean of concentrations measured from healthy microbialite periphyton. RA and RB are from the experiments conducted in 2021, in a flowing channel vs. microbialite interior, respectively. RC is from the experiment conducted in 2022 in a reef interior site where salinity reached halite saturation by day 72.

https://doi.org/10.1371/journal.pwat.0000100.g009

Community analysis from DNA sequencing. DNA sequencing results from the 2021 experiment indicated a consistent shift in community composition over time driven largely by a relative increase in Proteobacteria and Bacterioidota in bacterial 16S sequences (Fig 10A), and an increase in diatoms in eukaryotic 18S sequences (Fig 10B).

The community composition of control samples from a microbialite with a healthy periphyton was largely consistent with compositions found at other times and locations [12, 14], and distinctly different from the composition found on the t_0 control microbialite used to seed the experiments (Fig 10). The difference between healthy periphyton and t_0 control was especially apparent in the 18S results, where the healthy periphyton control samples were dominated by *Artemia* sequences, which were absent from the bleached t_0 control microbialite and early recovery experiment samples, as well as from water compositions at different points during the experiment. Principal components ordinate analysis using unweighted UniFrac sample distances indicated that the shift in recovery community was *away* from the healthy periphyton community, and more similar to water than healthy periphyton (Fig 10C and 10D). Amplicon sequence variant (ASV) tables of sequence abundance in each sample can be found in the OSF archive.

Analysis of cyanobacterial sequences. Cyanobacterial sequence abundance was low overall in our samples, likely the result of incomplete extraction, as cyanobacteria appeared to dominate sample biomass in microscopic examination (this is a commonly-reported issue for some cyanobacteria, especially in extreme environments [46, 47]). DNA sequencing of the V4 region of the 16S rRNA gene produced a total of 14 ASVs representing 9 genera classified as belonging to the phylum Cyanobacteria, of which 10 were classified as belonging to the phylogenetic

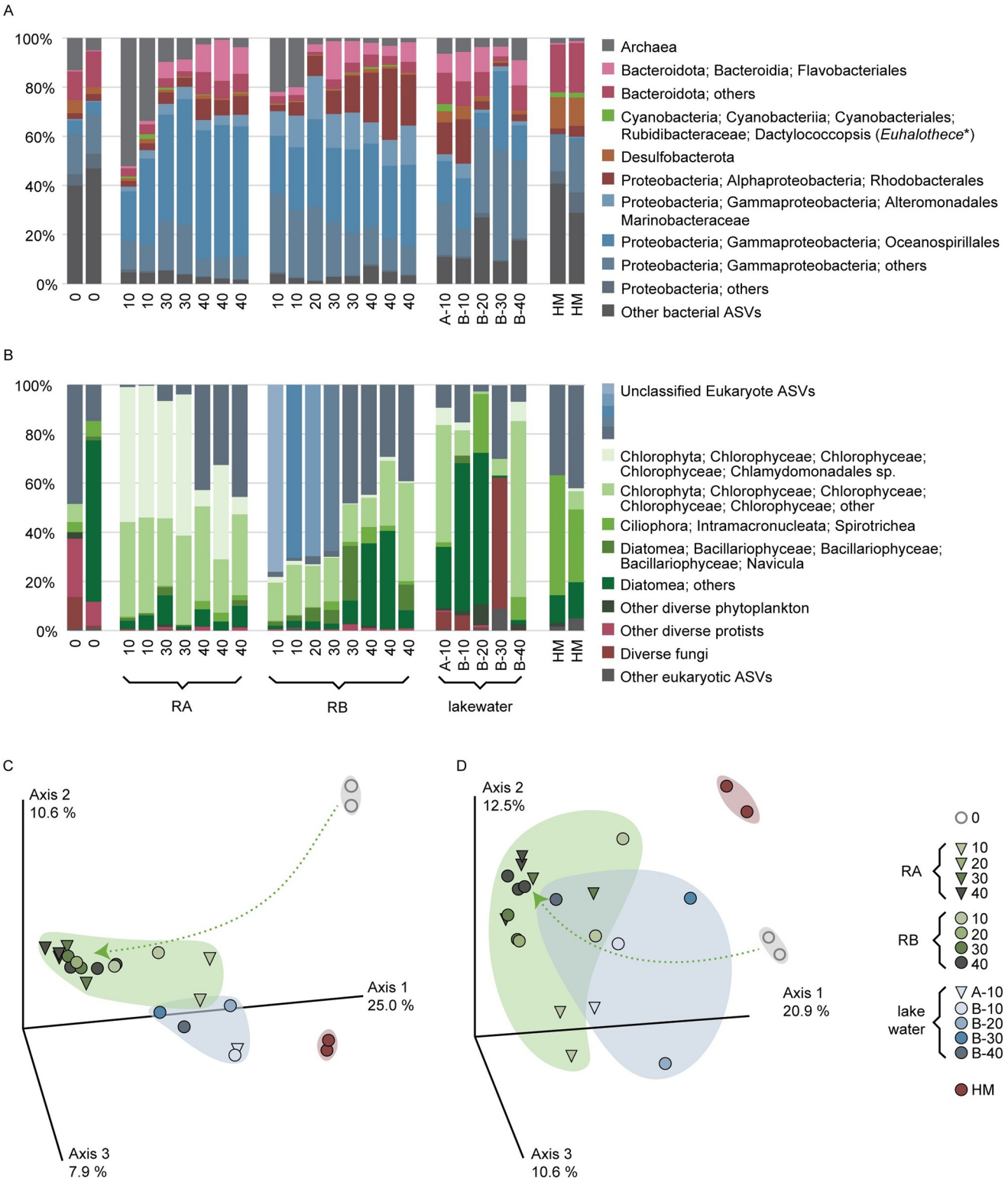

Fig 10. Recovery experiment DNA sequencing results. Results of 16S and 18S amplicon sequencing for the 2021 experiment at sites RA and RB, showing changes in microbial community over incubation time (numbers indicate incubation days) compared to lakewater and healthy microbialite periphyton (HM) samples. (A) Relative abundance of 16S sequencing ASVs belonging to different taxonomic groupings within the Bacteria and Archaea. *Most ASVs classed as *Dactylococcopsis* had closest sequence similarity to *Euhalothece*. (B) Relative abundance of 18S sequencing ASVs belonging to different taxonomic groupings within the Eukarya after contaminant, vertebrata, and arthropoda sequences were removed. (C) 16S and (D) 18S principal coordinate analysis

(PCoA) plots of unweighted UniFrac sample distances showing the grouping of like samples (green = recovery experiment samples, blue = lakewater samples, red = healthy microbialite periphyton samples, gray = desiccated t_0 control samples) and the evolution of the recovery experiment communities over time (green arrows) away from the healthy periphyton community. The percentages of sample variance explained by each of the three displayed axes are shown next to the respective axis. For interactive versions of these plots, the reader is directed to the qiime2 visualization files in the OSF archive, which can be viewed using the QIIME 2 View web interface (https://view.qiime2.org.

https://doi.org/10.1371/journal.pwat.0000100.g010

grouping of oxygenic photosynthetic cyanobacteria *sensu* Garcia-Pichel et al. [48], the others belonging to non-photosynthetic phyla. The greatest diversity in cyanobacterial sequences was found in lakewater samples. The desiccated t_0 control microbialite samples yielded no photosynthetic cyanobacterial ASVs; only one of the two replicates contained ASVs classified as belonging to the phylum Cyanobacteria, and those ASVs belonged to the Melainabacteria, a non-photosynthetic basal lineage [49, 50].

A narrow phylogenetic cluster of three ASVs classified as *Dactylococcopsis* against the SILVA 138 database [51] dominated the healthy microbialite and recovery samples (Fig S1.6 in S1 Appendix and S2 File), making up >94% of cyanobacterial sequences in the dataset, and 100% of sequences in most recovery samples. This cluster will be referred to as *Euhalothece* for the remainder of this paper [52, 53]. *Euhalothece* ASVs were relatively abundant in the control sample from a microbialite with a healthy periphyton, were present in some of the lakewater samples, absent in the desiccated t_o control sample, and appeared on recovery samples from both sites RA and RB by day 10.

The most abundant *Euhalothece* ASV (ASV1) had 100% sequence identity to several isolates of extremely halotolerant *Euhalothece* in the GenBank database [52, 54], including the strain MPI 96N304 (AJ000713.1) mentioned in Lindsay et al. [29]. ASV1 was found in the healthy microbialite samples, all recovery experiment samples, and most lakewater samples. A second ASV (ASV2), which differed by only one base pair from ASV1 (Table S1.5 in S1 Appendix), represented 41–50% of the cyanobacterial sequences in the healthy microbialite periphyton control samples, but was only found in the healthy microbialite samples—not in lakewater or recovery experiment samples. A third ASV (ASV3) had 100% sequence identity over the region sequenced to Great Salt Lake *Cyanothece* sp. GSL007 (FJ546715.1), as well as several isolates of *Dactylococcopsis salina* isolated from salt pans in Salin de Giraud, France [55], and uncultured clones from Guerrero Negro, Mexico [56]. ASV3 made up between 6–25% of cyanobacterial sequences in five of seven Site RA recovery samples, and was only found in the Site RA recovery samples—not in healthy microbialite samples, lakewater, Site RB recovery experiment samples.

Discussion

Microbialite bleaching is initially superficial, with some endoliths persisting over months of subaerial exposure

Although decreases in surface coloration were observed over a several week period (Fig 6), with a white zone of bleaching extending gradually downward on the microbialites (Fig 3 and S2 Fig), pigment extracts and microscopy from core samples revealed that bleaching was initially superficial, with substantial pigmented cellular material, including large *Euhalothece* clumps, persisting even in the upper ~1 cm samples (Fig 7 and S3 Fig).

Both our lab experiments and field observations indicate that some apparent bleaching, especially during early weeks of exposure, is attributable to the precipitation of reflective evaporite minerals on microbialite surfaces during subaerial exposure and evaporation. This is particularly obvious during periods of higher wave action, which can lead to the growth of mm-scale halite crystals on microbialite surfaces (Fig 5C). These minerals can dissolve during rain

events, leading to a significant re-greening of microbialites that previously appeared bleached (Figs 5 and 8, and S2 Fig).

Maintenance of chlorophyll *a* cm within the sampled microbialites (Fig 7A) may indicate an endolithic survival strategy during subaerial exposure. Survival of ordinarily surficial cyanobacteria and affiliated communities in the subsurface of permeable rock during periods of subaerial exposure has been documented in other systems, including desiccated lakes [57], and extracellular polymeric substances (EPS) can aid in desiccation and freezing survival in endolithic communities [58]. This is the first time to our knowledge that this growth habit has been documented in the Great Salt Lake microbialites; indeed, we are unaware of other literature documenting the impacts of subaerial exposure on microbialites over time periods longer than tidal cycles (e.g., [59]).

However, the fraction of DAPI-fluorescent cells decreased significantly over time at all sampled depths in the microbialite (up to the 4 cm depth monitored; Fig 7B), indicating that endolithic survival was not universal. Although it is not possible to tell from microscopy alone which taxa persisted or were lost, it appears from the chlorophyll results to be primarily non-photosynthetic members of the community, e.g., heterotrophs, sulfur cyclers, protists, fungi, and other diverse organisms, some of which may contribute to EPS production, overall biofilm structure, and nutrient cycling.

Microbialite bleaching enhances weathering

In longer-term observations of individual microbialites, substantial weathering was observed following periods of bleaching (Figs 3 and 6, S1 and S2 Figs). Upper portions of the microbialites lose their robust, gooey/blubber-like quality over periods of prolonged exposure and become loose and sandy, likely the direct consequence of declines in the surface microbial community and its affiliated EPS. Observable decreases in calcein fluorescence (Fig 7C), which binds to extracellular calcium and can therefore highlight degrading EPS, is consistent with this interpretation. The sandy carbonate material left on the desiccated surface is then easily weathered, as observed in the field and as illustrated in the observed mass loss following rinse events during the lab desiccation experiments (Fig 8). Enhanced weathering of the microbialites may be one of the longer-lasting consequences of microbialite exposure, as microbialite growth rates are not yet known in Great Salt Lake, but assumed to be quite slow [21].

Partial recovery of bleached microbialites occurs even at high salinity levels

The results of our recovery experiments in summer/autumn 2021 were broadly encouraging, showing an exponential rate of recovery when desiccated samples were re-submerged in lakewater at a salinity between 13–17%, as measured by extractable chlorophyll *a* and DNA (Fig 9A and 9B). If recovery continued along the same exponential trajectory observed over the initial 40 days of the experiment, a full recovery to "healthy" values could occur within 130 days of being re-submerged, i.e., a single summer growth season (Fig 9C and 9D). Also encouraging was the appearance of *Euhalothece* sequences on the recovery samples after just 10 days incubation, as well as sequences of eukaryotic phototrophs (Fig 10A and 10B). The combined results imply that a recovery of the ecosystem-critical microbialite primary producers is possible if microbialites—even badly bleached microbialites—are re-submerged in healthy lakewater. However, as discussed in the next section, while *Euhalothece* (and, thus, chlorophyll and presumably primary productivity) return to the microbialites, we did not see evidence of the return of the full, healthy microbial community in our analysis of the DNA sequencing data; thus, the time and conditions to true recovery (full-community and robust microbial mat) remains uncertain.

When we repeated the experiment in the higher-salinity water of summer–autumn, 2022 (18–27%), recovery was markedly slower (with a calculated doubling time from chlorophyll recovery of 31 days vs. 9 and 16 days at the two 2021 sites, although the exponential best fit was poor in 2022) but did eventually appear to occur, with extracted chlorophyll *a* values reaching those seen in 2021 by 72 days incubation, and increasing further in the following month (Fig 9A). *Euhalothece* clumps were visible in microscopic analyses in samples collected after 2–3 months incubation (S3 Fig), supplying additional evidence of recovery. This is remarkable, considering the salinity was at or near halite saturation when this apparent recovery was occurring. It is possible that the apparent recovery was simply a gradual accumulation of cells from the surrounding water (supported by the faster recovery rates of microbialites exposed to more lakewater flow; Fig 9A and 9B), which could potentially be preserved for some time by encrusting halite [60]. Additional work is required to determine whether the observed *Euhalothece* are actually photosynthetically active, or simply preserved.

Microbialite recolonization likely depends on the health of the lakewater community

Recovery of the microbialite communities in our 2021 experiment (no DNA sequencing results are available for the 2022 experiments) appears to be based on recolonization from the surrounding water, rather than a 'resurrection' of dormant endolithic communities. Community distance analysis indicates that the microbial community present in recovery samples were more similar to lakewater than to either the desiccated microbialite t_0 community or the community present on microbialites with healthy periphyton (Fig 10C and 10D). The recovery sample communities that are most similar to lakewater were unsurprisingly those incubated for the shortest periods, and evolved away from lakewater over time, suggesting an initial seeding by lakewater. It is also notable that the 2021 recovery experiment site located in a channel away from the greater reef and exposed to more water flow (Site RA) experienced recovery rates that were nearly twice as fast as was seen at the reef-interior site (Site RB) despite similar salinity levels and hydrologic connection.

The recovery sample community also evolved over time to become *less* similar to that seen in microbialites with healthy periphyton, despite the persistence of *Euhalothece*. Most notable is the relative dearth of Desulfobacterota in recovery experiment samples and high abundance of Flavobacteriales, Rhodobacterales, and Gammaproteobacteria, especially Marinobacteraceae and Oceanospirillales (Fig 10A and 10B). The low abundance of Desulfobacteria can be explained by the high salinity levels present during the recovery experiments; even halotolerant strains are not known to tolerate salinity levels above 13% [61, 62]. It could, however, also be a consequence of an immature microbial mat lacking the anoxic zones required to support sulfur-reducing metabolisms. What is unclear is whether—given enough time and development of a robust biofilm, then microbial mat—the community would begin to shift to more closely resemble that seen in microbialites with a healthy periphyton.

Primary seeding from lakewater indicates that microbialite recolonization is dependent on the health of the lakewater microbial ecosystem and the presence of viable *Euhalothece* and other organisms in lakewater. While microbialite communities may be able to survive, or at least be preserved, through periods of subaerial exposure and at high salinity, this is not true of lakewater communities. In the north arm of Great Salt Lake, where salinity values routinely exceed 24%, *Euhalothece* sequences are absent [29], and the community composition is markedly different than that in the lake's south arm. Thus, a high-salinity lake would not be able to re-seed healthy microbialite periphyton communities. It appears that the lake's south arm is the ultimate reservoir for the organisms and metabolisms that support the broader Great Salt Lake ecosystem, including the microbialite microbial communities.

Conclusions

Great Salt Lake's microbialites and their surface microbial communities are in peril from declining lake water levels and a concurrent increase in the salinity of the lake, which is amplified in hydrologically closed areas of microbialite reef. In recent years, dramatic bleaching of newly-exposed microbialites has been observed, causing concern about the future of the microbialites and impacts on the broader ecosystem. Here, we have shown that microbialite bleaching is initially superficial, with an endolithic survival mode allowing the microbialite communities to be resilient for months after surface bleaching is observed. We also showed that portions of the microbialite surface communities, including the ecosystem-critical cyanobacterial component, begin to recover when bleached, desiccated microbialites are re-submerged and seeded by healthy lakewater communities. In other words, if lake level rebounds, microbialite periphyton communities and their ecosystem function could potentially recover (Fig 11).

However, microbialite surface communities are not quite "just add water" communities: to re-seed, they require the right water, consisting of a healthy microbial community, which necessitates salinity levels that are lower than what is anticipated if lake level continues to fall or if freshwater input remains low. In addition, prolonged periods of subaerial exposure result in enhanced weathering of the microbialites, brushing off carbonate growth that may have taken centuries to form, and shrinking the overall height and surface area of these structures. This could have consequences for productivity in an otherwise healthy lake: less microbialite surface area means less area that can host productive periphyton, and less area on which brine fly larvae can anchor.

Much remains to be elucidated in this system. Can re-submerged microbialites make a full recovery, and how long does it take? What are the conditions under which recovery can occur? Is the persistence of chlorophyll and DNA several cm deep within the microbialite indicative of a healthy endolithic community, or simply preservation in halite? Which microbialite residents are truly critical to support the greater Great Salt Lake ecosystem? Are more ancient layers of the microbialite more resistant to weathering? And if so, what processes led to their more robust lithification that are different from what we have seen since the last time the microbialites were exposed *en masse*?

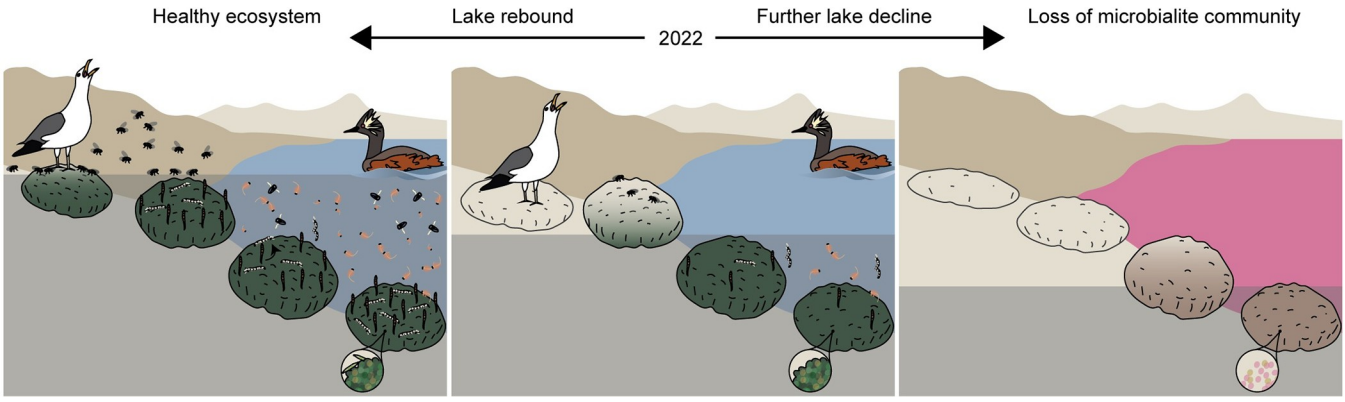

Fig 11. Summary of the big-picture findings of this study. The left panel shows a healthy Great Salt Lake ecosystem at an elevation of roughly 1279 m, where microbialites are mostly submerged and salinity levels are moderate. The center panel shows the state of the lake in summer–autumn 2022, when ~40% of microbialite reef area was subaerially exposed and salinity was high, resulting in a substantial decrease in the health and productivity of microbialite periphyton and reduced brine fly pupae anchor sites, as well as weathering of exposed microbialites. The right panel illustrates a potential future where lake levels continue to decline and salinity continues to increase, similar to what is seen in the modern north arm of the lake, where microbialites no longer support a healthy, productive periphyton and other key members of the ecosystem are absent due to exceeded salinity thresholds. Rapid lake rebound could result in the recovery of the microbialite-supported ecosystem so long as salinity levels do not preclude the survival of recolonizing organisms.

https://doi.org/10.1371/journal.pwat.0000100.g011

The message of this study is a hopeful, yet urgent one: if changes in human water use can result in more freshwater flowing back into the lake soon, we can still expect to see a recovery of microbialite-supported primary productivity in Great Salt Lake. However, if lake level continues to decline, producing further increases in lake salinity prior to a rebound in lake level, desiccated microbialites may not re-seed with their chief primary producers. Indeed, microbialites in the salt-saturated north arm of Great Salt Lake no longer support a cyanobacterial periphyton [29]. Meanwhile, the longer already-exposed microbialites remain exposed, the more they will weather, potentially decreasing their future capacity to contribute to the Great Salt Lake ecosystem. Thus, the time to act is now.

Even more broadly, this study highlights the urgency of threats of desiccation and salinity rise faced by saline lake ecosystems worldwide, which house organisms that, while remarkable in their ability to survive extreme conditions, have limits. In this case, a single year and lake elevation change of ~1 m hurtled Great Salt Lake toward an ecological tipping point that threatened part of the base of the lake's hemispherically-important food chain. Such tipping points, as in this case, may not be characterized until they are reached or exceeded. The ecosystem support role of microbialites in other modern ecosystems, especially systems threatened by modern environmental change, warrants further research.

Supporting information

S1 Appendix. Supplemental information. Includes supplemental methods, with additional details for microbialite surface color band measurements, the recovery experiment field setup, lab desiccation experiment lamps, CLSM settings, image analysis protocols, and DNA extraction, amplification, sequencing, and analysis protocols. Also includes an analytical discussion of different methods for salinity measurements, methods for assessing microbialite health, core data ANOVA, and an analysis of cyanobacterial sequences. Additional supporting files archived in Open Science Framework are also described.
(DOCX)

S1 Fig. Time series field photographs of monitored microbialites. Time series photomicrographs showing the initial stages of bleaching of several different microbialites over time. Numbers represent the number of days the microbialites were subaerially exposed when the photo was taken. All microbialites shown were located near Site B3. (A) Microbialite M6, (B) Microbialite M5, and (C) Microbialite M13 monitored in July–August 2021. (D) Microbialite M1, (E) Microbialite M2, and (F) Microbialite M3 monitored in July–August 2022. Features of note include bright gray halite mineral formation visible in the latter panels of A & B and the 14-day panels of E–F, weathering in the 13-day panel of C, and re-greening following rain events in the 21-day panels of E–F.
(TIF)

S2 Fig. Microbialite surface color band layer measurements. Summary illustration of surface observations of microbialite bleaching and weathering, showing measurements of changing heights of surficial microbialite color bands (and the total height of microbialites above the surrounding sediment) over a four-week period. Areas outlined in white bars represent actual band location measurements and measured microbialite heights at each of four timepoints, plotted as the average of multiple measurements from each of four microbialites. Measurements are based on the vertical distance from the water surface at the time of measurement, corrected for fluctuating lake level and presented as height above the approximate location of the soft sediment surrounding the microbialites. Error bars represent the standard deviation of twelve measurements for a single color band and indicate the approximate error range for all bands. White dots indicate the measured water level at Site B3. Bands above the white dots are

subaerial, while bands below the white circles are submerged, overlaid by water depth at Site B3 (white line). Colors represent the approximate color of the observed bands. Values plotted are averages of multiple measurements from four microbialites. Error bars represent the standard deviation of twelve measurements for a single color band and indicate the approximate error range for all bands.
(TIF)

S3 Fig. Representative brightfield photomicrographs from core and recovery experiment samples at Site B3. Panel columns represent different sample types: (A) microbialite core top (horizon T) samples, (B) microbialite core bottom (horizon B) samples, and (C) recovery experiment samples. Panel rows indicate the collection date: Samples were collected from microbialite cores at Site B3 on July 12 (day 0; left column of images), August 2 (day 21; center column of images), and September 22 (day 72; right column of images), 2022. Each row of images contains representative photomicrographs from a different core horizon taken at each date. (A) Microbialite core top (horizon T) section samples. (B) Microbialite core bottom (horizon B) section samples. (C) Recovery experiment samples. In all images, the scale bar represents 100 μm. All images were manually adjusted for consistent white balance.
(TIF)

S1 Table. Field sites. Locations referred to in this paper, including sampling locations and logger sites.
(XLSX)

S2 Table. Time series data summary. Daily time series data for lake elevation, weather, and water temperature, light, and salinity. Condenses the full-resolution timeseries dataset available in the OSF archive.
(XLSX)

S3 Table. Microbialite surface color band and % green measurements. Measurements of color band locations on monitored microbialites, and % green values calculated from photographs of microbialites M1–M3.
(XLSX)

S4 Table. Lab desiccation experiment results. Measurements of surface %green and mass from the lab microbialite desiccation experiment.
(XLSX)

S1 File. Microscopy and extract results. Sample information and measurements of extractable DNA, calculated chlorophyll *a* concentrations, and color analyses for brightfield and confocal microscopy. Includes measurements from microbialite cores and recovery experiment samples. Summarizes the full raw datasets available in the OSF archive.
(XLSX)

S2 File. Recovery experiment 16S and 18S sequencing results. Relative abundance of dominant taxa found in 16S and 18S sequences used to generate the bar plots in Fig 10. Also includes the cyanobacterial ASV table used for Fig S1.6 in S1 Appendix. Summarizes the full ASV tables available in the OSF archive.
(XLSX)

Acknowledgments

Sampling at Great Salt Lake was done under Utah Department of Natural Resources permit #410–00736 and equivalent earlier permits, as well as a MOU with Antelope Island State Park,

which also provided access to KUTSYRAC22 weather data. KUTSYRAC27 weather station data was obtained with permission from the owners (Thompson family). We acknowledge the use of imagery from the NASA Worldview application (https://worldview.earthdata.nasa.gov), part of the NASA Earth Observing System Data and Information System (EOSDIS). Microbialite color band measurements reported in this study were done by Jared Gibby. We gratefully acknowledge instrumentation support at Weber State from Leigh Komperda, Elizabeth Sandquist, Michele Culumber, and Marek Matyjasik, logistical support from Ross LaRue, and administrative support from Ana Cich. CF would also like to acknowledge the numerous Weber State undergraduate student researchers, past and present, who inspired and informed early work that led to the projects presented here, especially Celina Patiño, Charise Penrod, and Aybree DeGrange.

Author Contributions

Conceptualization: Carie Frantz.

Data curation: Carie Frantz.

Formal analysis: Carie Frantz, Cecilia Gibby, Rebekah Nilson, Maggie Nguyen, Cody Ellsworth, Hank Dolan, Alvin Sihapanya, Jake Aeschlimann.

Funding acquisition: Carie Frantz, Bonnie K. Baxter.

Investigation: Carie Frantz, Rebekah Nilson, Cole J. Stern, Maggie Nguyen, Cody Ellsworth.

Methodology: Carie Frantz, Cecilia Gibby, Rebekah Nilson, Cole J. Stern, Maggie Nguyen, Cody Ellsworth.

Project administration: Carie Frantz.

Resources: Carie Frantz.

Software: Carie Frantz.

Supervision: Carie Frantz, Bonnie K. Baxter.

Validation: Carie Frantz, Cecilia Gibby, Rebekah Nilson.

Visualization: Carie Frantz, Cole J. Stern, Alvin Sihapanya, Jake Aeschlimann.

Writing – original draft: Carie Frantz, Cecilia Gibby, Rebekah Nilson.

Writing – review & editing: Carie Frantz, Cecilia Gibby, Cole J. Stern, Hank Dolan, Alvin Sihapanya, Jake Aeschlimann, Bonnie K. Baxter.

References

1. Wurtsbaugh WA, Miller C, Null SE, DeRose RJ, Wilcock P, Hahnenberger M, et al. Decline of the world's saline lakes. Nat Geosci. 2017; 10: 816–821. https://doi.org/10.1038/ngeo3052
2. Hassani A, Azapagic A, D'Odorico P, Keshmiri A, Shokri N. Desiccation crisis of saline lakes: A new decision-support framework for building resilience to climate change. Sci Total Environ. 2020; 703: 134718. https://doi.org/10.1016/j.scitotenv.2019.134718 PMID: 31734504
3. Wurtsbaugh WA, Sima S. Contrasting Management and Fates of Two Sister Lakes: Great Salt Lake (USA) and Lake Urmia (Iran). Water. 2022; 14: 3005. https://doi.org/10.3390/w14193005
4. WHSRN. Great Salt Lake—Western Hemisphere Shorebird Reserve Network. In: Great Salt Lake [Internet]. 9 Jan 2023 [cited 3 Feb 2023]. Available: https://whsrn.org/whsrn_sites/great-salt-lake/
5. Conover MR, Bell ME. Importance of Great Salt Lake to Pelagic Birds: Eared Grebes, Phalaropes, Gulls, Ducks, and White Pelicans. In: Baxter BK, Butler JK, editors. Great Salt Lake Biology: A Terminal Lake in a Time of Change. Cham: Springer International Publishing; 2020. pp. 239–262. https://doi.org/10.1007/978-3-030-40352-2_8

6. Sorensen ED, Hoven HM, Neill J. Great Salt Lake Shorebirds, Their Habitats, and Food Base. In: Baxter BK, Butler JK, editors. Great Salt Lake Biology: A Terminal Lake in a Time of Change. Cham: Springer International Publishing; 2020. pp. 263–309. https://doi.org/10.1007/978-3-030-40352-2_9

7. Marden B, Brown P, Bosteels T. Great Salt Lake Artemia: Ecosystem Functions and Services with a Global Reach. In: Baxter BK, Butler JK, editors. Great Salt Lake Biology: A Terminal Lake in a Time of Change. Cham: Springer International Publishing; 2020. pp. 175–237. https://doi.org/10.1007/978-3-030-40352-2_7

8. Domagalski JL, Orem WH, Eugster HP. Organic geochemistry and brine composition in Great Salt, Mono, and Walker Lakes. Geochim Cosmochim Acta. 1989; 53: 2857–2872.

9. Jones BF, Naftz DL, Spencer RJ, Oviatt CG. Geochemical Evolution of Great Salt Lake, Utah, USA. Aquat Geochem. 2009; 15: 95–121. https://doi.org/10.1007/s10498-008-9047-y

10. Vennin E, Bouton A, Bourillot R, Pace A, Roche A, Brayard A, et al. The lacustrine microbial carbonate factory of the successive Lake Bonneville and Great Salt Lake, Utah, USA. Brasier A, editor. Sedimentology. 2019; 66: 165–204. https://doi.org/10.1111/sed.12499

11. Chidsey TC, Vanden Berg MD, Eby DE. Petrography and characterization of microbial carbonates and associated facies from modern Great Salt Lake and Uinta Basin's Eocene Green River Formation in Utah, USA. Geol Soc Lond Spec Publ. 2015; 418: 261–286. https://doi.org/10.1144/SP418.6

12. Ingalls M, Frantz CM, Snell KE, Trower EJ. Carbonate facies-specific stable isotope data record climate, hydrology, and microbial communities in Great Salt Lake, UT. Geobiology. 2020; 18: 566–593. https://doi.org/10.1111/gbi.12386 PMID: 32196875

13. Baskin RL, Della Porta G, Wright VP. Characteristics and controls on the distribution of sublittoral microbial bioherms in Great Salt Lake, Utah: Implications for understanding microbialite development. Depositional Rec. 2022; 8: 39–66. https://doi.org/10.1002/dep2.159

14. Kanik M, Munro-Ehrlich M, Fernandes-Martins MC, Payne D, Gianoulias K, Keller L, et al. Unexpected Abundance and Diversity of Phototrophs in Mats from Morphologically Variable Microbialites in Great Salt Lake, Utah. Atomi H, editor. Appl Environ Microbiol. 2020; 86: e00165–20. https://doi.org/10.1128/AEM.00165-20 PMID: 32198176

15. Wang S-Y, Gillies RR, Jin J, Hipps LE. Coherence between the Great Salt Lake Level and the Pacific Quasi-Decadal Oscillation. J Clim. 2010; 23: 2161–2177. https://doi.org/10.1175/2009JCLI2979.1

16. Williams AP, Cook ER, Smerdon JE, Cook BI, Abatzoglou JT, Bolles K, et al. Large contribution from anthropogenic warming to an emerging North American megadrought. Science. 2020; 368: 314–318. https://doi.org/10.1126/science.aaz9600 PMID: 32299953

17. Null SE, Wurtsbaugh WA. Water Development, Consumptive Water Uses, and Great Salt Lake. In: Baxter BK, Butler JK, editors. Great Salt Lake Biology: A Terminal Lake in a Time of Change. Cham: Springer International Publishing; 2020. pp. 1–21. https://doi.org/10.1007/978-3-030-40352-2_1

18. Hassan D, Burian SJ, Johnson RC, Shin S, Barber ME. The Great Salt Lake Water Level is Becoming Less Resilient to Climate Change. Water Resour Manag. 2022 [cited 31 Jan 2023]. https://doi.org/10.1007/s11269-022-03376-x

19. Abbott BW, Baxter BK, Busche K, de Freitas L, Frei R, Gomez T, et al. Emergency measures needed to rescue Great Salt Lake from ongoing collapse. Provo, Utah: Brigham Young University; 2023 Jan p. 34. Available: https://pws.byu.edu/great-salt-lake

20. Bouton A, Vennin E, Boulle J, Pace A, Bourillot R, Thomazo C, et al. Linking the distribution of microbial deposits from the Great Salt Lake (Utah, USA) to tectonic and climatic processes. Biogeosciences. 2016; 13: 5511–5526. https://doi.org/10.5194/bg-13-5511-2016

21. Newell DL, Jensen JL, Frantz CM, Vanden Berg MD. Great Salt Lake (Utah) Microbialite $\delta^{13}C$, $\delta^{18}O$, and $\delta^{15}N$ Record Fluctuations in Lake Biogeochemistry Since the Late Pleistocene. Geochem Geophys Geosystems. 2017; 18: 3631–3645. https://doi.org/10.1002/2017GC007078

22. DeMott LM, Scholz CA, Awaleh MO. Lacustrine carbonate towers of Lake Abhe, Djibouti: Interplay of hydrologic and microbial processes. Sediment Geol. 2021; 424: 105983. https://doi.org/10.1016/j.sedgeo.2021.105983

23. López-García P, Kazmierczak J, Benzerara K, Kempe S, Guyot F, Moreira D. Bacterial diversity and carbonate precipitation in the giant microbialites from the highly alkaline Lake Van, Turkey. Extremophiles. 2005; 9: 263–274. https://doi.org/10.1007/s00792-005-0457-0 PMID: 15959626

24. Smith MD, Goater SE, Reichwaldt ES, Knott B, Ghadouani A. Effects of recent increases in salinity and nutrient concentrations on the microbialite community of Lake Clifton (Western Australia): are the thrombolites at risk? Hydrobiologia. 2010; 649: 207–216. https://doi.org/10.1007/s10750-010-0246-3

25. Akkuş M, Sarı M, Ekmekçi FG, Yoğurtçuoğlu B. The discovery of a microbialite-associated freshwater fish in the world's largest saline soda lake, Lake Van (Turkey). Zoosystematics Evol. 2021; 97: 181–189. https://doi.org/10.3897/zse.97.62120

26. Rishworth GM, Dodd C, Perissinotto R, Bornman TG, Adams JB, Anderson CR, et al. Modern supratidal microbialites fed by groundwater: functional drivers, value and trajectories. Earth-Sci Rev. 2020; 210: 103364. https://doi.org/10.1016/j.earscirev.2020.103364

27. Falace A, Bressan G. 'Periphyton' Colonization: Principles, Criteria and Study Methods. In: Jensen AC, Collins KJ, Lockwood APM, editors. Artificial Reefs in European Seas. Dordrecht: Springer Netherlands; 2000. pp. 435–449. https://doi.org/10.1007/978-94-011-4215-1_26

28. Pace A, Bourillot R, Bouton A, Vennin E, Galaup S, Bundeleva I, et al. Microbial and diagenetic steps leading to the mineralisation of Great Salt Lake microbialites. Sci Rep. 2016; 6: 31495. https://doi.org/10.1038/srep31495 PMID: 27527125

29. Lindsay MR, Anderson C, Fox N, Scofield G, Allen J, Anderson E, et al. Microbialite response to an anthropogenic salinity gradient in Great Salt Lake, Utah. Geobiology. 2017; 15: 131–145. https://doi.org/10.1111/gbi.12201 PMID: 27418462

30. Wurtsbaugh WA, Gardberg J, Izdepski C. Biostrome communities and mercury and selenium bioaccumulation in the Great Salt Lake (Utah, USA). Sci Total Environ. 2011; 409: 4425–4434. https://doi.org/10.1016/j.scitotenv.2011.07.027 PMID: 21835437

31. Anderson NL, Barrett KL, Jones SE, Belovsky GE. Impact of abiotic factors on microbialite growth (Great Salt Lake, Utah, USA): a tank experiment. Hydrobiologia. 2020; 847: 2113–2122. https://doi.org/10.1007/s10750-020-04235-9

32. Collins N. Population ecology of Ephydra cinerea Jones (Diptera: Ephydridae), the only benthic metazoan of the Great Salt Lake, U.S.A. Hydrobiologia. 1980; 68: 99–112. https://doi.org/10.1007/BF00019696

33. Barrett KL. Microbialite communities and food web linkages in Great Salt Lake. Notre Dame. 2020.

34. Caudell JN, Conover MR. Energy content and digestibility of brine shrimp (*Artemia franciscana*) and other prey items of eared grebes (*Podiceps nigricollis*) on the Great Salt Lake, Utah. Biol Conserv. 2006; 130: 251–254. https://doi.org/10.1016/j.biocon.2005.12.018

35. Belovsky GE, Stephens D, Perschon C, Birdsey P, Paul D, Naftz D, et al. The Great Salt Lake Ecosystem (Utah, USA): long term data and a structural equation approach. Ecosphere. 2011; 2: art33. https://doi.org/10.1890/ES10-00091.1

36. Brown PD, Craine JM, Richards D, Chapman A, Marden B. DNA metabarcoding of the phytoplankton of Great Salt Lake's Gilbert Bay: Spatiotemporal assemblage changes and comparisons to microscopy. J Gt Lakes Res. 2022; 48: 110–124. https://doi.org/10.1016/j.jglr.2021.10.016

37. Baskin RL. Occurrence and Spatial Distribution of Microbial Bioherms in Great Salt Lake, Utah. Doctoral Dissertation, University of Utah. 2014.

38. U.S. Geological Survey. USGS Water Data for the Nation. 2022 [cited 31 Jan 2023]. Available: https://waterdata.usgs.gov/nwis

39. Walters W, Hyde ER, Berg-Lyons D, Ackermann G, Humphrey G, Parada A, et al. Improved Bacterial 16S rRNA Gene (V4 and V4-5) and Fungal Internal Transcribed Spacer Marker Gene Primers for Microbial Community Surveys. mSystems. 2015; 1: e00009–15. https://doi.org/10.1128/mSystems.00009-15 PMID: 27822518

40. Amaral-Zettler LA, McCliment EA, Ducklow HW, Huse SM. A Method for Studying Protistan Diversity Using Massively Parallel Sequencing of V9 Hypervariable Regions of Small-Subunit Ribosomal RNA Genes. Langsley G, editor. PLoS ONE. 2009; 4: e6372. https://doi.org/10.1371/journal.pone.0006372 PMID: 19633714

41. Stoeck T, Bass D, Nebel M, Christen R, Jones MDM, Breiner H-W, et al. Multiple marker parallel tag environmental DNA sequencing reveals a highly complex eukaryotic community in marine anoxic water. Mol Ecol. 2010; 19: 21–31. https://doi.org/10.1111/j.1365-294X.2009.04480.x PMID: 20331767

42. Bolyen E, Rideout JR, Dillon MR, Bokulich NA, Abnet CC, Al-Ghalith GA, et al. Reproducible, interactive, scalable and extensible microbiome data science using QIIME 2. Nat Biotechnol. 2019; 37: 852–857. https://doi.org/10.1038/s41587-019-0209-9 PMID: 31341288

43. Naftz DL, Millero FJ, Jones BF, Green WR. An Equation of State for Hypersaline Water in Great Salt Lake, Utah, USA. Aquat Geochem. 2011; 17: 809–820. https://doi.org/10.1007/s10498-011-9138-z

44. Roberts E, Kroker J, Körner S, Nicklisch A. The role of periphyton during the re-colonization of a shallow lake with submerged macrophytes. Hydrobiologia. 2003; 506: 525–530. https://doi.org/10.1023/B:HYDR.0000008560.73832.1c

45. Fischer M, Friedrichs G, Lachnit T. Fluorescence-Based Quasicontinuous and In Situ Monitoring of Biofilm Formation Dynamics in Natural Marine Environments. Appl Environ Microbiol. 2014; 80: 3721–3728. https://doi.org/10.1128/AEM.00298-14 PMID: 24727266

46. Garcia-Pichel F, López-Cortés A, Nübel U. Phylogenetic and Morphological Diversity of Cyanobacteria in Soil Desert Crusts from the Colorado Plateau. Appl Environ Microbiol. 2001; 67: 1902–1910. https://doi.org/10.1128/AEM.67.4.1902-1910.2001 PMID: 11282648

47. Bernardo, Alcántara-Hernández RJ, Montejano G, López-Martínez R, Falcón LI, Becerra-Absalón I. Cyanobacteria in microbialites of Alchichica Crater Lake: a polyphasic characterization. Eur J Phycol. 2021; 56: 428–443. https://doi.org/10.1080/09670262.2020.1853815

48. Garcia-Pichel F, Zehr JP, Bhattacharya D, Pakrasi HB. What's in a name? The case of cyanobacteria. J Phycol. 2020; 56: 1–5. https://doi.org/10.1111/jpy.12934 PMID: 31618454

49. Di Rienzi SC, Sharon I, Wrighton KC, Koren O, Hug LA, Thomas BC, et al. The human gut and groundwater harbor non-photosynthetic bacteria belonging to a new candidate phylum sibling to Cyanobacteria. Kolter R, editor. eLife. 2013; 2: e01102. https://doi.org/10.7554/eLife.01102 PMID: 24137540

50. Soo RM, Hemp J, Parks DH, Fischer WW, Hugenholtz P. On the origins of oxygenic photosynthesis and aerobic respiration in Cyanobacteria. Science. 2017; 355: 1436–1440. https://doi.org/10.1126/science.aal3794 PMID: 28360330

51. Yilmaz P, Parfrey LW, Yarza P, Gerken J, Pruesse E, Quast C, et al. The SILVA and "All-species Living Tree Project (LTP)" taxonomic frameworks. Nucleic Acids Res. 2014; 42: D643–D648. https://doi.org/10.1093/nar/gkt1209 PMID: 24293649

52. Garcia-Pichel F, Nübel U, Muyzer G. The phylogeny of unicellular, extremely halotolerant cyanobacteria. Arch Microbiol. 1998; 169: 469–482. https://doi.org/10.1007/s002030050599 PMID: 9575232

53. Margheri MC, Ventura S, Kaštovský J, Komárek J. The taxonomic validation of the cyanobacterial genus Halothece. Phycologia. 2008; 47: 477–486. https://doi.org/10.2216/07-87.1

54. Sayers EW, Bolton EE, Brister JR, Canese K, Chan J, Comeau DC, et al. Database resources of the national center for biotechnology information. Nucleic Acids Res. 2022; 50: D20–D26. https://doi.org/10.1093/nar/gkab1112 PMID: 34850941

55. Hamlaoui S, Yéprémian C, Duval C, Marie B, Djédiat C, Piquet B, et al. The Culture Collection of Cyanobacteria and Microalgae at the French National Museum of Natural History: A Century Old But Still Alive and Kicking! Including in Memoriam: Professor Alain Couté. Cryptogam Algol. 2022; 43: 41–83. https://doi.org/10.5252/cryptogamie-algologie2022v43a3

56. Kirk Harris J, Gregory Caporaso J, Walker JJ, Spear JR, Gold NJ, Robertson CE, et al. Phylogenetic stratigraphy in the Guerrero Negro hypersaline microbial mat. ISME J. 2013; 7: 50–60. https://doi.org/10.1038/ismej.2012.79 PMID: 22832344

57. Sánchez-Sánchez J, Cerca M, Alcántara-Hernández RJ, Lozano-Flores C, Carreón-Freyre D, Levresse G, et al. Extant microbial communities in the partially desiccated Rincon de Parangueo maar crater lake in Mexico. FEMS Microbiol Ecol. 2019; 95: fiz051. https://doi.org/10.1093/femsec/fiz051 PMID: 31055602

58. Knowles EJ, Castenholz RW. Effect of exogenous extracellular polysaccharides on the desiccation and freezing tolerance of rock-inhabiting phototrophic microorganisms: Effect of EPS on tolerance of rock-inhabiting phototrophs. FEMS Microbiol Ecol. 2008; 66: 261–270. https://doi.org/10.1111/j.1574-6941.2008.00568.x PMID: 18710394

59. Wong HL, Smith D-L, Visscher PT, Burns BP. Niche differentiation of bacterial communities at a millimeter scale in Shark Bay microbial mats. Sci Rep. 2015; 5: 15607. https://doi.org/10.1038/srep15607 PMID: 26499760

60. Perl SM, Baxter BK. Great Salt Lake as an Astrobiology Analogue for Ancient Martian Hypersaline Aqueous Systems. In: Baxter BK, Butler JK, editors. Great Salt Lake Biology: A Terminal Lake in a Time of Change. Cham: Springer International Publishing; 2020. pp. 487–514. https://doi.org/10.1007/978-3-030-40352-2_16

61. Brandt KK, Ingvorsen K. Desulfobacter halotolerans sp. nov., a Halotolerant Acetate-Oxidizing Sulfate-Reducing Bacterium Isolated from Sediments of Great Salt Lake, Utah. Syst Appl Microbiol. 1997; 20: 366–373. https://doi.org/10.1016/S0723-2020(97)80004-5

62. Qian Z, Tianwei H, Mackey HR, van Loosdrecht MCM, Guanghao C. Recent advances in dissimilatory sulfate reduction: From metabolic study to application. Water Res. 2019; 150: 162–181. https://doi.org/10.1016/j.watres.2018.11.018 PMID: 30508713

63. Baxter B. Great Salt Lake microbiology: a historical perspective. International Microbiology. 2018; 21: 79–95. https://doi.org/10.1007/s10123-018-0008-z PMID: 30810951